European Journal of Medicinal Chemistry 253 (2023) 115305

Contents lists available at ScienceDirect

European Journal of Medicinal Chemistry

journal homepage: www.elsevier.com/locate/ejmech

Research paper

Discovery of a potent and selective allosteric inhibitor targeting the SHP2 tunnel site for RTK-driven cancer treatment

Ruixiang Luo [a,1], Weitao Fu [b,1], Jingjing Shao [a,c,1], Lin Ma [a,1], Sujuan Shuai [d], Ying Xu [a], Zheng Jiang [a], Zenghui Ye [a], Lulu Zheng [e], Lei Zheng [a], Jie Yu [a], Yawen Zhang [a], Lina Yin [a], Linglan Tu [a], Xinting Lv [a], Jie Li [a,d,***], Guang Liang [a,c,**], Lingfeng Chen [a,*]

[a] Affiliated Yongkang First People's Hospital and School of Pharmacy, Hangzhou Medical College, Hangzhou, Zhejiang, 310012, China
[b] Department of Computer-Aided Drug Design, Jiangsu Vcare PharmaTech Co. Ltd., Nanjing, 211800, China
[c] School of Pharmaceutical Sciences, Wenzhou Medical University, Wenzhou, Zhejiang, 325035, China
[d] Department of Pharmacy, School of Medicine, Zhejiang University City College, Hangzhou, 310015, China
[e] Department of Pharmacy, Tongde Hospital of Zhejiang Province, Hangzhou, Zhejiang, 310000, China

ARTICLE INFO

Keywords:
SHP2
Receptor tyrosine kinase
Lead compound
Structure-based virtual screening
Structure-activity relationship

ABSTRACT

Src homology 2 domain-containing phosphatase 2 (SHP2) is a cytoplasmic protein tyrosine phosphatase (PTP) that regulates signal transduction of receptor tyrosine kinases (RTKs). Abnormal SHP2 activity is associated with tumorigenesis and metastasis. Because SHP2 contains multiple allosteric sites, identifying inhibitors at specific allosteric binding sites remains challenging. Here, we used structure-based virtual screening to directly search for the SHP2 "tunnel site" allosteric inhibitor. A novel hit (70) was identified as the SHP2 allosteric inhibitor with an IC_{50} of 10.2 μM against full-length SHP2. Derivatization of hit compound 70 using molecular modeling-guided structure-based modification allowed the discovery of an effective and selective SHP2 inhibitor, compound 129, with 122-fold improved potency compared to the hit. Further studies revealed that 129 effectively inhibited signaling in multiple RTK-driven cancers and RTK inhibitor-resistant cancer cells. Remarkably, 129 was orally bioavailable ($F = 55\%$) and significantly inhibited tumor growth in haematological malignancy. Taken together, compound 129 developed in this study may serve as a promising lead or candidate for cancers bearing RTK oncogenic drivers and SHP2-related diseases.

1. Introduction

The SHP2 protein is a well-validated oncogenic protein tyrosine phosphatase (PTP) [1]. This non-receptor type PTP is universally expressed and functions as a signal transducer in multiple cancer-related signaling pathways, including the Ras-Raf-extracellular-signal-regulated kinase (ERK), Janus kinase (JAK)-signal transducer and activator of transcription (STAT), and Nuclear factor (NF)-κB cascades [2]. Furthermore, SHP2 participated in programmed cell death protein 1 (PD-1) immune checkpoint signaling and contributes to immune evasion [3]. Abnormal SHP2 activation has been linked to developmental diseases [4,5] and functions as an oncogenic driver in cancer patients, including those with solid tumors and hematologic cancers [6,7]. SHP2 genetic knockdown or pharmacological inhibition blocks RAS/MAPK signaling and suppresses RTKs-driven cancer cell proliferation [8]. Hence, SHP2 is an attractive target for cancer therapeutics.

The SHP2 structure comprises of two SH2 domains and a PTP domain that governs dephosphorylation activity (Fig. 1A) [9]. In the auto-inhibited conformation, the N-SH2 region of SHP2 interacts with the PTP region, thereby blocking the substrate binding [9]. Upon substrate phosphotyrosine (pTyr) binding, SHP2 enters the activated state by exposing the catalytic site of the PTP domain [10]. Owing to this unique feature, both orthostatic and allosteric inhibitors have been identified. Orthostatic SHP2 inhibitors (e.g., NSC-87877 [11] and NAT6-297775 [6]) directly bind to the active site of the PTP domain and suppress enzymatic activity. However, potent SHP2 orthostatic inhibitor

* Corresponding author. School of Pharmaceutical Sciences, Hangzhou Medical College, Hangzhou, 310012, China.
** Corresponding author. School of Pharmaceutical Sciences, Hangzhou Medical College, Hangzhou, 310012, China.
*** Corresponding author. School of Pharmaceutical Sciences, Zhejiang University City College, Hangzhou, 310015, China.
E-mail addresses: lijie@zucc.edu.cn (J. Li), wzmcliangguang@163.com (G. Liang), lfchen@hmc.edu.cn (L. Chen).
[1] These authors contributed equally to this work.

https://doi.org/10.1016/j.ejmech.2023.115305
Received 13 January 2023; Received in revised form 14 March 2023; Accepted 22 March 2023
Available online 24 March 2023

development is challenging owing to the extremely conserved polar character of the catalytic site [12]. Currently, allosteric inhibitors are promising regarding use in clinical studies. Therefore, identifying druggable SHP2 allosteric sites and novel allosteric inhibitors presents a major direction in SHP2-targeted studies.

Currently, multiple potential allosteric inhibitor binding sites of SHP2 have been identified, including the tunnel, latch, and groove binding sites formed between the SH2 and PTP domain interface (Fig. 1B) [13]. To identify SHP2 allosteric inhibitors, experimental high-throughput screening (HTS) protocols were previously performed. For instance, a diverse library of 100,000 molecules was screened using the 6,8-difluoro-4-methylumbelliferyl phosphate (DiFMUP) biochemical assay in the presence of a pIRS-1 activating peptide. The first pyrazin-core-based allosteric inhibitor, SHP099, was discovered by HTS, which inspired the structure-based development of novel SHP2 allosteric inhibitors (Fig. 1C) [2]. In the past five years, a series of SHP099 derivatives, namely TNO155 [14], RMC-4630 [8], and JAB-3068 [15] have entered clinical trials for cancer therapy. These allosteric SHP2 inhibitors are inserted into the central tunnel pocket, where they function as a 'molecular glue' to stabilize the inactive state of SHP2. Furthermore, a triazolo–quinazolinone-core-based compound, SHP244 [13], functions as a distinct allosteric inhibitor by occupying the latch binding site (Fig. 1C).

Despite the development of HTS biochemical assays, several issues remain regarding the identification of SHP2 allosteric hits. Firstly, considerable amounts of small molecule compound libraries are required for experimental screening, which in turn results in high time consumption and economic costs. Secondly, initial hit compounds require further profilization against the PTP domain of SHP2 (SHP2-PTP) to deprioritize orthostatic SHP2 inhibitors and enrich the allosteric site inhibitors. Thirdly, multiple allosteric pockets complicate allosteric inhibitor identification at specific desired sites. For instance, to screen non-tunnel site allosteric inhibitors, a special screening paradigm was developed by Fodor et al. [13]. Three rounds of sequential HTS against the wild-type SHP2, SHP2-PTP, and SHP2$^{T253M/Q257L}$ (tunnel site blocked mutant) enzymes were conducted sequentially (Fig. 1C). Lastly, additional X–ray crystallography is typically employed to resolve any unknown binding modes, considering the occurrence of various potential allosteric pockets (Fig. 1C).

To effectively identify new SHP2 allosteric inhibitors that specifically target the tunnel site, a multistep structure-based virtual screening (SBVS) approach was designed and used to predict potential hits directly targeting the tunnel site of SHP2 (Fig. 1D). Compared with experimental HTS, SBVS presents several advantages, such as improved economic and time costs, as well as higher hit rates [16,17]. Here, a new hit compound 70, containing a pyrimidine-5-carboxamide core, was validated as a novel SHP2 inhibitor that binds to the tunnel site. Molecular modeling-guided structure optimization combined with a two-round structure-activity relationship (SAR) analysis of compound 70 revealed a potent and selective "tunnel site" inhibitor, compound 129. To our best knowledge, it is the first time to discover allosteric inhibitor of SHP2 tunnel site through direct virtual screening. We further evaluate the anti-cancer effects of compound 129 both *in vitro* and in *vivo*, and identify compound 129 as a valuable candidate for SHP2-related disease treatment.

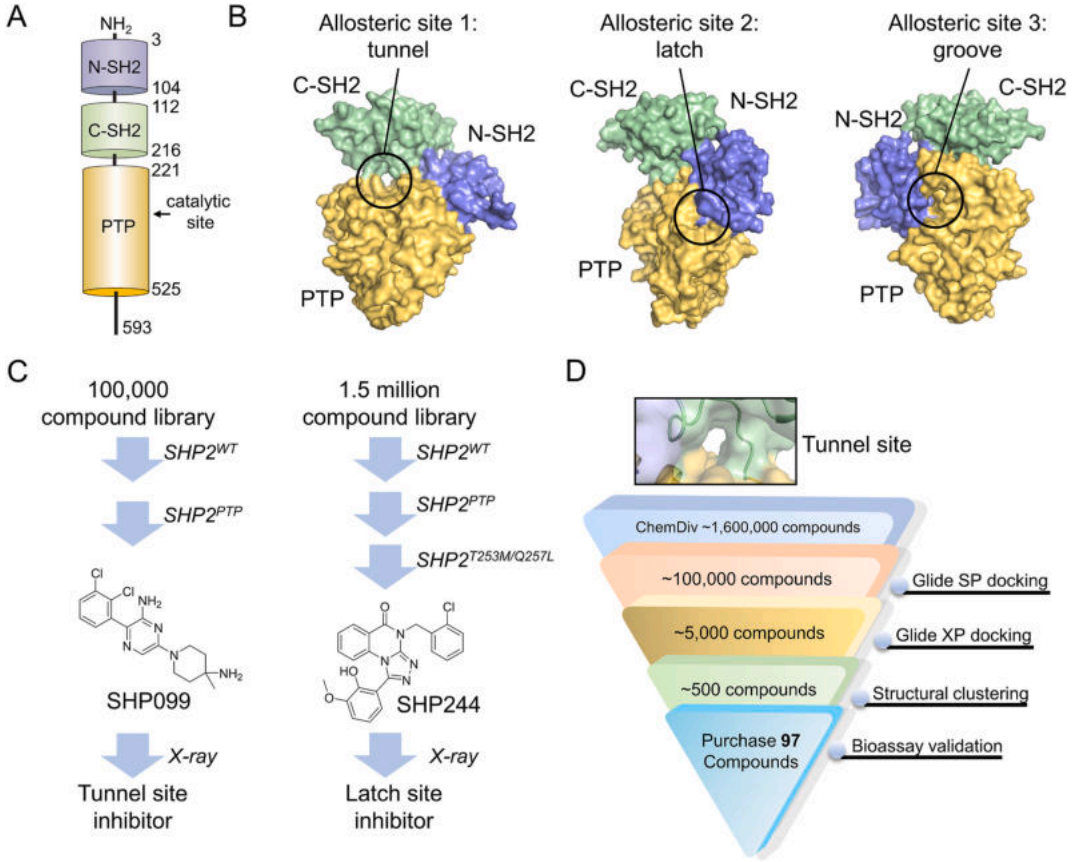

Fig. 1. Structure-based virtual screening (SBVS) for SHP2 tunnel site allosteric inhibitors. (A) Schematic illustration of SHP2 domains containing N-SH2 (blue), C-SH2 (green), and protein tyrosine phosphatase (PTP) domain (yellow). (B) Three predicted allosteric pockets of the autoinhibited conformation of SHP2 including tunnel, latch, and groove sites. (C) Screening paradigm of reported allosteric inhibitors discovery yielding SHP099 and SHP244. (D) Schematic workflow of SBVS used in present study.

2. Results

2.1. Hit compound 70 is a novel SHP2 allosteric inhibitor

The SBVS workflow used in this project is shown in Fig. 1D. We started with 1.6 million small-molecule compounds from the ChemDiv library using our previously reported strategy [18,19]. By filtering Lipinski's rule of five, cascade molecular docking, and structural clustering, 97 potential SHP2 tunnel site allosteric inhibitors were selected and subjected to DiFMUP biochemical assays (Fig. 2A, structures listed in Table S1). As shown in Fig. 2B, three initial hits with distinct scaffolds: 4358-1548 (4, quinolin-4-amine core), M503-0874 (70, phenylpyrimidine-5-carboxamide core), and S634-1472 (84, pyrrole-3-carboxamide core), showed inhibitory rates of >60%. The IC_{50} values of these three compounds were 13.5, 10.2, and 19.0 μM, respectively. For the following study, compound 70 was selected for further study based on the lower IC_{50} and favored pyrimidine core for SHP2 tunnel site. The dose-response DiFMUP assays for 70 are shown in Fig. 2C.

To verify the allosteric binding sites of 70, a tunnel site binding-deficient SHP2 mutant ($SHP2^{T253M/Q257L}$) was constructed, which significantly abolished the activity of 70 (Fig. 2D), revealing that the

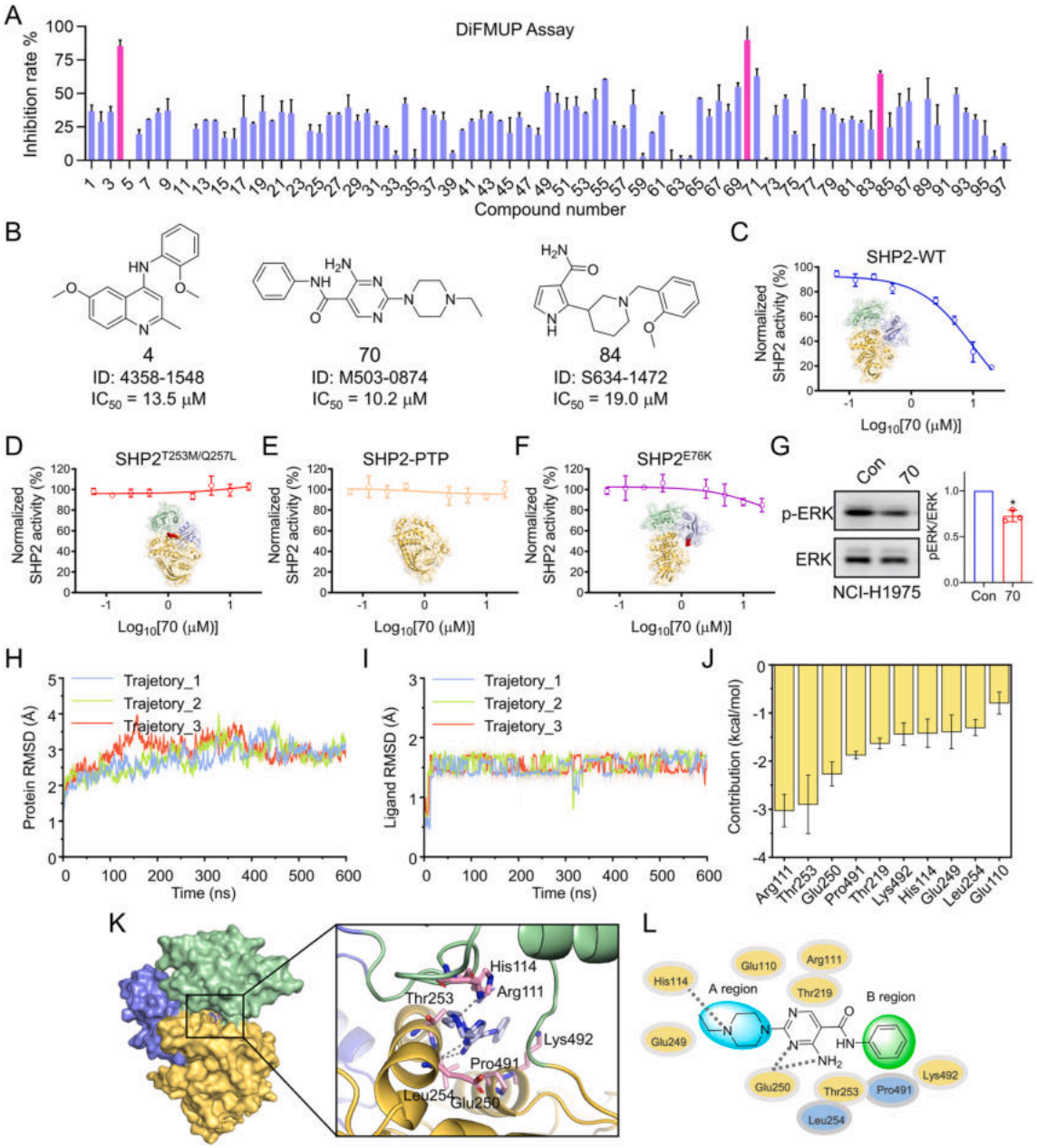

Fig. 2. Discovery of a hit compound 70 as a novel SHP2 allosteric inhibitor. (A) Drug screening for 97 compounds selected by structure based virtual screening (SBVS) via 6,8-difluoro-4-methylumbelliferyl phosphate (DiFMUP) assay. Compounds with inhibition rates >60% threshold at 20 μM are highlighted in purple. (B) Chemical structures and IC_{50} values of hit compounds 4, 70, and 84. (C–F) Dose-response DiFMUP assays for compound 70 with $SHP2^{WT}$ (C), $SHP2^{T253M/Q257L}$ (D), SHP2-PTP (E), and $SHP2^{E76K}$ (F). (G) Western blot of p-ERK from H1975 cells treated with 10 μM compound 70. (H) Molecular dynamics (MD) simulation analysis of compound 70 bound to the SHP2 tunnel site. Root mean square deviation (RMSD) curves for the SHP2 protein backbone C_α atoms during three parallel 600 ns MD simulations. (I) RMSD curves for 70 heavy atoms during three parallel 600 ns MD simulations. (J) Top 10 predicted key residues for the binding of compound 70 to SHP2 (Mean ± standard deviation [SD]). (K) Three-dimensional (3D) representation of the key residues for 70 bound to SHP2. (L) Top 10 residues for 70 bound to SHP2 in two-dimensional (2D) representation.

T253 M/Q257L mutation disrupted the direct interaction between 70 and the SHP2 tunnel site. Additionally, 70 showed no inhibition against truncated SHP2 (SHP2-PTP) or the oncogenic mutant of $SHP2^{E76K}$; the latter variant induced SH2 domain reorganization and tunnel site diminishing (Fig. 2E and F) [20]. These experimental data consistently confirmed the molecular mechanism of 70 by binding to the SHP2 tunnel site and stabilizing the inactive form of the SHP2. To further validate the potency of SHP2 inhibition in cells, compound 70 was used to treat NSCLC cell line (NCI–H1975) with abnormal epidermal growth factor receptor (EGFR) alterations. As shown in Fig. 2G, treatment with 70 at 10 μM concentration led to a modest reduction in ERK phosphorylation. Altogether, compound 70 serves as a novel SHP2 inhibitor and is a promising starting point for structural optimization.

2.2. Binding mode analysis of compound 70 in the SHP2 tunnel site

To further guide compound 70 structural optimization, the binding pose of 70 bound to the SHP2 tunnel site extracted from SBVS was subjected to three parallel 600 ns molecular dynamics (MD) simulations to explore the dynamic behavior. As shown in Fig. 2H, the RMSDs of the protein backbone C_α atoms of SHP2 tended to converge after approximately 200 ns of MD simulation with RMSD fluctuations of <2 Å. Those for the heavy atoms of 70 were only after approximately 25 ns of MD simulations with RMSD fluctuations of <1 Å (Fig. 2I). The results indicated that compound 70 could stably bind to the "tunnel" binding site of SHP2. Additionally, we obtained a series of dynamic structures of SHP2-70 complexes for the subsequent energetic and structural analysis. To highlight the residues contributing to the binding of 70 to SHP2, per-residue decompositions were calculated based on a modified MM/GBSA method named the variable atomic dielectric-MM/GBSA (VAD-MM/GBSA) method, as previously reported [21]. By directly assigning variable dielectric constants to the protein/ligand atoms, the VAD-MM/GBSA method improved the accuracy of binding affinity calculations compared to the conventional MM/GBSA method [21]. As shown in Fig. 2J, the predicted top-ranked residues for the binding of 70 to SHP2 were Arg111, Thr253, Glu250, Pro491, Thr219, Lys492, His114, Glu249, Leu254, and Glu110 (Fig. 2J). Structural analysis of these key residues indicated that hydrophilic interactions and hydrogen bonds involving residues His144 and Glu250 dominantly contributed to 70 binding to the SHP2 tunnel site (Fig. 2K-L). With the binding information of hit 70 in mind, we decided to maintain the central pyrimidine-5-carboxamide core and independently evaluate the SAR of the ethylpiperazin (A region) followed by phenyl (B region) groups.

2.3. SAR study of the A region

SAR study of the ethylpiperazin motif, which occupies the solvent-exposed polar region within the allosteric pocket formed by residues His114, Thr218, Glu249, and Glu250. Twenty analogs of compound 70 were purchased from the ChemDiv chemical library or synthesized for *in vitro* biochemical assays (Table 1). First, we introduced hydrophobic substituents on the piperazine ring, such as propyl (98) and isopropyl (99), which did not affect dephosphorylation activity. This activity was slightly improved by the introduction of an acetyl group (100). In contrast, further extension of the acetyl group (101–103) resulted in lower potency. Similarly, incorporation of phenyl (105), methoxyphenyl (106), pyridine (107), or cyclohexyl (108) moieties at the same site of piperazin also abolished potency, suggesting that bulky substitution on piperazine may not be tolerated at the tunnel site. Transforming the piperazine motif with other rings, including thiomorpholine (109), morpholine (110), piperidines (111–114), and pyrrolidine (115), significantly affects the SHP2 inhibitory activity. Among which, the incorporation of 4-aminopiperidine (112) and 4-ethoxycarbonyl-piperidine (113) motif improved the SHP2 inhibition activity by 7-and 5-fold, respectively (112: IC_{50} = 1.4 μM; 113: IC_{50} = 2.1 μM). Interestingly, the replacement of the ethylpiperazin motif with aliphatic chains or benzene rings significantly decreased the inhibition potency.

2.4. SAR study of the B region

Next, we focused on the *N*-phenyl ring (Table 2), which occupies the hydrophobic region of the allosteric binding pocket formed by residues Thr253, Leu254, and Pro491. Compound 112, with relatively high activity, was selected for further modification. First, we explored the effect

Table 1
Structure-activity relationship (SAR) study of the A region.

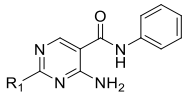

Comp.	R_1	SHP2 IC_{50} (μM)	Comp.	R_1	SHP2 IC_{50} (μM)	Comp.	R_1	SHP2 IC_{50} (μM)
70		10.2 ± 2.5	104	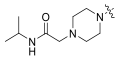	5.6 ± 1.7	111		12.8 ± 1.7
98		11.5 ± 3.0	105		>100	112		1.4 ± 0.5
99		9.3 ± 2.7	106	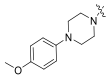	>100	113	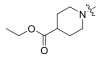	2.1 ± 0.7
100		6.7 ± 1.9	107		>100	114		>100
101	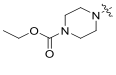	8.5 ± 2.2	108		>100	115		50 ± 15
102	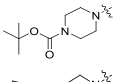	35 ± 10	109		5.6 ± 1.2	116		25 ± 16
103	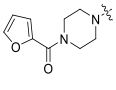	>100	110		9.5 ± 4.5	117		>100
						SHP099		0.089 ± 0.023

Table 2
Structure-activity relationship (SAR) study of the B region.

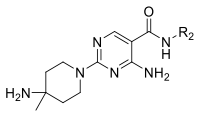

Comp.	R_2	SHP2 IC_{50} (μM)	Comp.	R_2	SHP2 IC_{50} (μM)	Comp.	R_2	SHP2 IC_{50} (μM)
112		1.4 ± 0.7	122		1.9 ± 1.1	127		0.25 ± 0.22
118		>100	123		2.3 ± 1.8	128		3.4 ± 2.0
119		8.0 ± 3.3	124		12.5 ± 4.3	129		0.083 ± 0.019
120		>100	125		2.0 ± 0.8	130		8.1 ± 3.7
121		>100	126		0.62 ± 0.30	131		0.80 ± 0.24
						SHP099		0.075 ± 0.015

of phenyl arrangements on the activity and replaced the phenyl with naphthalen (118–119), biphenyl (120), and fluoren (121) moieties. SAR analysis indicated that the phenyl group was favored. We then introduced different substituents on the benzene ring (e.g., 122–128). The introduction of an electron-donating methoxy group did not further increase activity (122–124). By comparing the activities of compounds 125–128, we determined that the activity of the compound was slightly improved in the presence of halogen substitution at the para-position of the benzene ring (127: IC_{50} = 0.25 μM). Interestingly, when the phenyl group was replaced with pyridin-3-yl (129), the activity of the compound was greatly improved with IC_{50} value of 0.083 μM, which shows similar potency as reported inhibitor SHP099. While further attempts to reposition the pyridine of 129 or extend the pyridine group (130–131) resulted in a significant loss in phosphatase inhibition.

2.5. Binding mode analysis of compound 129 in the SHP2 tunnel site

MD simulations were applied to compound 129 bound to SHP2 to provide clues for the binding molecular mechanism. As shown in Fig. 3A and B, the RMSD curves of the SHP2 protein backbone C_α atoms tended to converge after approximately 150 ns MD simulations with RMSD fluctuations within 2 Å. Meanwhile, the RMSD curves of 129 heavy atoms were dynamically stable throughout the MD simulations, with RMSD fluctuations within 1 Å. The MD simulation results indicate that the binding between 129 and SHP2 was dynamically stable, and the trajectories were submitted for binding free energy calculations based

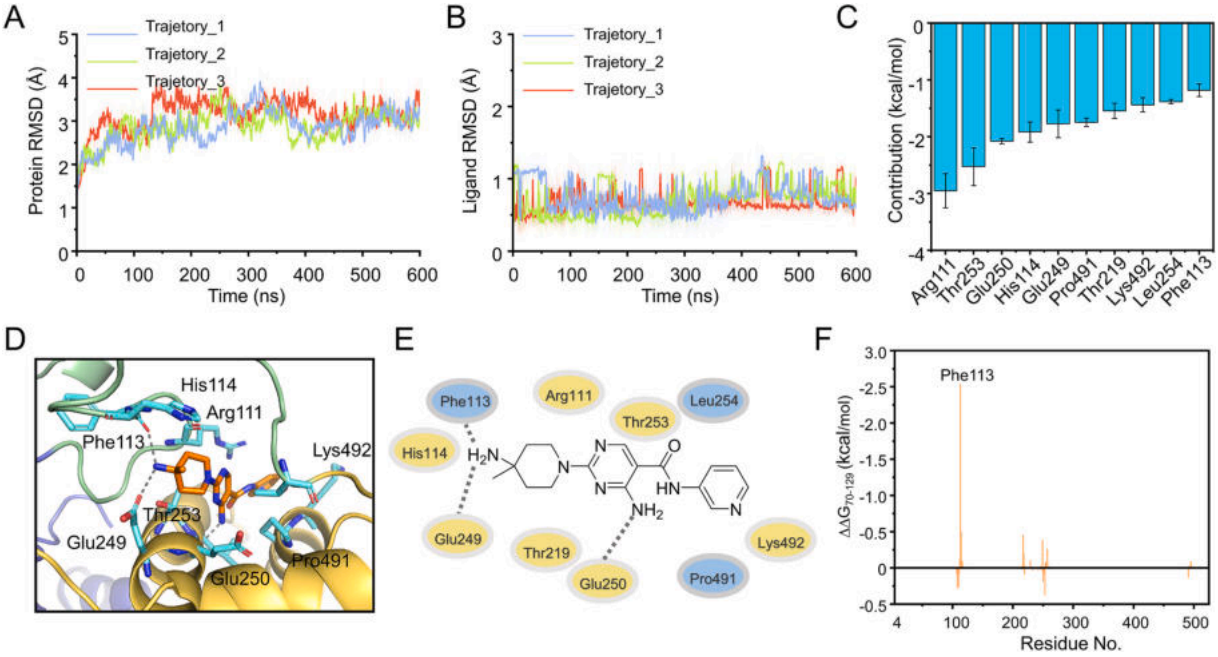

Fig. 3. Molecular dynamic (MD) simulation analysis of compound 129 bound to the SHP2 tunnel site. (A) Root mean square deviation (RMSD) curves for the SHP2 protein backbone C_α atoms during three parallel 600 ns MD simulations. (B) RMSD curves for 129 heavy atoms during three parallel 600 ns MD simulations. (C) Top 10 interacting residues for the binding of 129 to SHP2 (Mean ± standard deviation [SD]). (D) Three-dimensional (3D) representation of the key residues for compound 129 bound to SHP2. (E) Two-dimensional (2D) representation of the top 10 residues for compound 129 bound to SHP2. (F) Energy differences between compound 70 and 129 ($\Delta\Delta G = \Delta G_{70} - \Delta G_{129}$).

on the VD-MM/GBSA methods. As shown in Fig. 3C, the predicted top-ranked residues for binding of 129 to SHP2 were Arg111, Thr253, Glu250, His114, Glu249, Pro491, Thr219, Lys492, Leu254, and Phe113. Structural analysis indicated that hydrophilic interactions and hydrogen bonds involving residues Phe113 and Glu250 dominantly contributed to 129 the binding to the SHP2 tunnel site (Fig. 3D and E). Among these key residues, nine were the same as the key residues for 70 bound to SHP2. The energetic differences for each corresponding residue between 70 and 129 ($\Delta\Delta G = \Delta G_{70} - \Delta G_{129}$) were calculated to further highlight the energetic differences between them. The residues with positive values form stronger interactions with 129 than with 70, whereas the negative values indicate that the residues form better interactions with 70. Notably, most of SHP2 residues possess similar energetic contributions to compound 129 and 70. However, only Phe113 formed a much stronger interaction with compound 129 than with 70 (Fig. 3F). Structural investigation showed that a hydrogen bond was formed between Phe113 and 129, but not 70 (Fig. 2K–3L and Fig. 3D–4E).

Structural analysis indicated that 129 formed a much stronger interaction with Phe113 than with the lead compound 70. Interestingly, compared with compound 112, the introduction of the pyridine ring on 129 (B region) improved the inhibitory activity by 16-fold, but the underlying mechanism has not been solved by molecular simulation docking. Currently, co-crystallization of SHP2 and compound 129 is ongoing in our lab to further analyze the contribution of the pyridine ring to tunnel site binding.

2.6. *Active compound 129 inhibits pERK level and proliferation of RTK driven cancer cells*

In a previous study, we found that compound 129 possessed high inhibitory activity and selectivity for SHP2 *in vitro*. To further investigate whether compound 129 efficiently inhibited SHP2 at the cellular

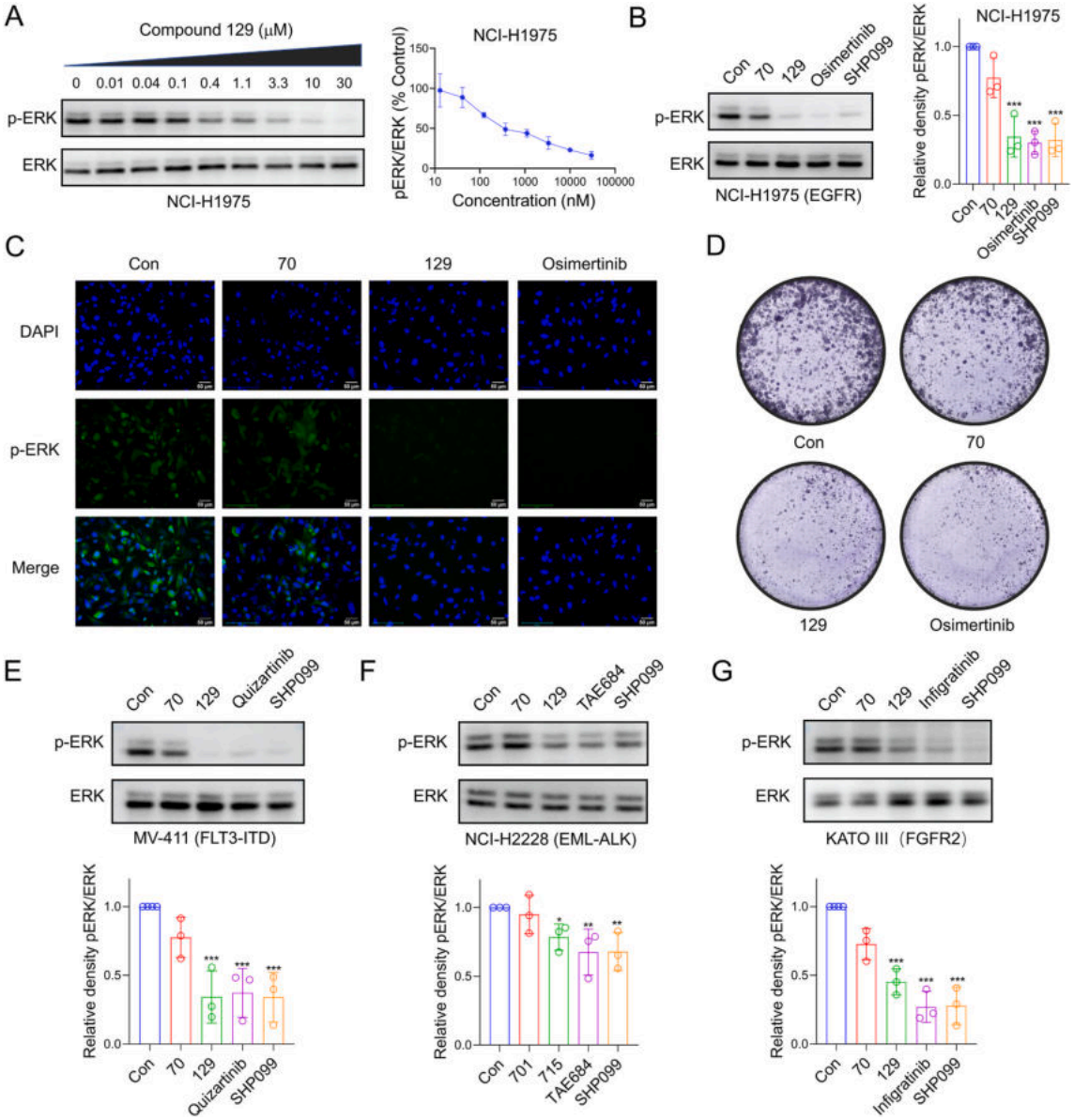

Fig. 4. Compound 129 inhibited pERK levels and receptor tyrosine kinase (RTK)-driven cancer cell proliferation. (A) pERK activity inhibition by increased concentration of compound 129 in NCI–H1975 cells assayed by Western blot. (B) p-ERK inhibition potency evaluation by compound 70, 129, osimertinib, and SHP099 at 10 μM in NCI–H1975 cells. (C) H1975 cells treated with compound 70, 129, or osimertinib were stained with DAPI and p-ERK antibodies. (D) Colony formation of H1975 in the presence of compound 70, 129, or osimertinib. (E–G) p-ERK inhibition potency evaluation by compound 70, 129, RTKi (quizartinib, TAE684, or infigratinib), and SHP099 at 10 μM in MV-411 (E), NCI–H2228 (F), and KATO III (G) cancer cells.

level, SHP2-dependent NSCLC cells were treated with increasing concentrations of compound 129 (0.01–30 μM). As shown in Fig. 4A, compound 129 suppressed the phosphorylation of ERK with an IC_{50} of 0.59 ± 0.28 μM in EGFR-driven NCI–H1975 cells. Compared to lead compound 70, 129 demonstrated greatly improved pERK inhibitory activity, which was comparable to that of the third-generation EGFR inhibitor osimertinib (Fig. 4B). The Western blot results were consistent with the p-ERK immunofluorescence and colony formation assays (Fig. 4C and D). To further validate the effects of compound 129 on other RTK-driven cancers, a cell-based study was extended to four additional SHP2-dependent cell lines with known alterations in oncogenic RTKs, including MV-411 (FLT3-ITD mutation), NCI–H2228 (EML-ALK fusion), and KATO III (FGFR2 amplification). As shown in Fig. 4E–G, 129 treatment resulted in significant pERK inhibition, as observed in all the RTK-driven cell lines, especially in hematopoietic cancer cells. 129 exhibited a pERK inhibitory effect comparable to that of the FLT3 inhibitor quizartinib.

2.7. Compound 129 inhibits pERK level in osimertinib-resistant NSCLC cells

Despite the therapeutic success of RTK inhibitors, acquired resistance remains a major clinical issue in patients. Thus, after verifying the inhibitory effect of compound 129 on different RTK-dependent tumor cells, we further explored whether compound 129 could effectively inhibit pERK signaling in RTKi-resistant cells. Previous studies have found that patients with NSCLC may develop acquired resistance after a period of osimeritinib use. The major drug resistance mechanisms include the EGFR C797S mutation in the kinase domain (EGFR-dependent) and the bypass activating mutation involving other RTKs (EGFR-independent) [22,23]. We assumed that NSCLC carrying these two RTK-related resistance mutations remains SHP2-dependent. To test this hypothesis, osimertinib-resistant NCI–H1975 cells (NCI–H1975-OR) were established. Indeed, as shown in Fig. 5A, compound 129 potently inhibit the pERK signaling in a dose-dependent manner with IC_{50} of 0.63 ± 0.32 μM, which is close to IC_{50} level of wild-type H1975 cells (0.59 μM). As predicted, 129 showed much higher pERK inhibitory potency than osimertinib against H1975-OR, as demonstrated by the immunofluorescence results (Fig. 5B). We also found that compound 129 cooperates with osimertinib to exert a synergistic effect (Fig. 5B).

2.8. Compound 129 inhibit SHP2 downsream signalling via disrupting SHP2 related protein association

Previous study indicated that SHP2 is essential to link RTKs and downstream signalling by forming the RTK-proximal complex (Fig. 6A). Thus, SHP2 inhibitor compound 129 may be able to disrupt the signalosome that is required for RTK activation. To test this hypothesis, we evaluated whether 129 affect the protein-protein-interaction of SHP2 with the universal scaffold protein of RTKs, GRB2- associated-binding protein 1 (GAB1) [24], in HEK293T cells. Indeed, through immunoprecipitation experiments, 129 treatment dismished SHP2's interaction with the adaptor protein GAB1, and showed much stronger effect compared to lead compound (Fig. 6B). Thus, allosteric inhibition of SHP2 by 129 could interfere with the signalosome formation assembled at RTKs via disruption of SHP2 associated adaptor proteins interactions.

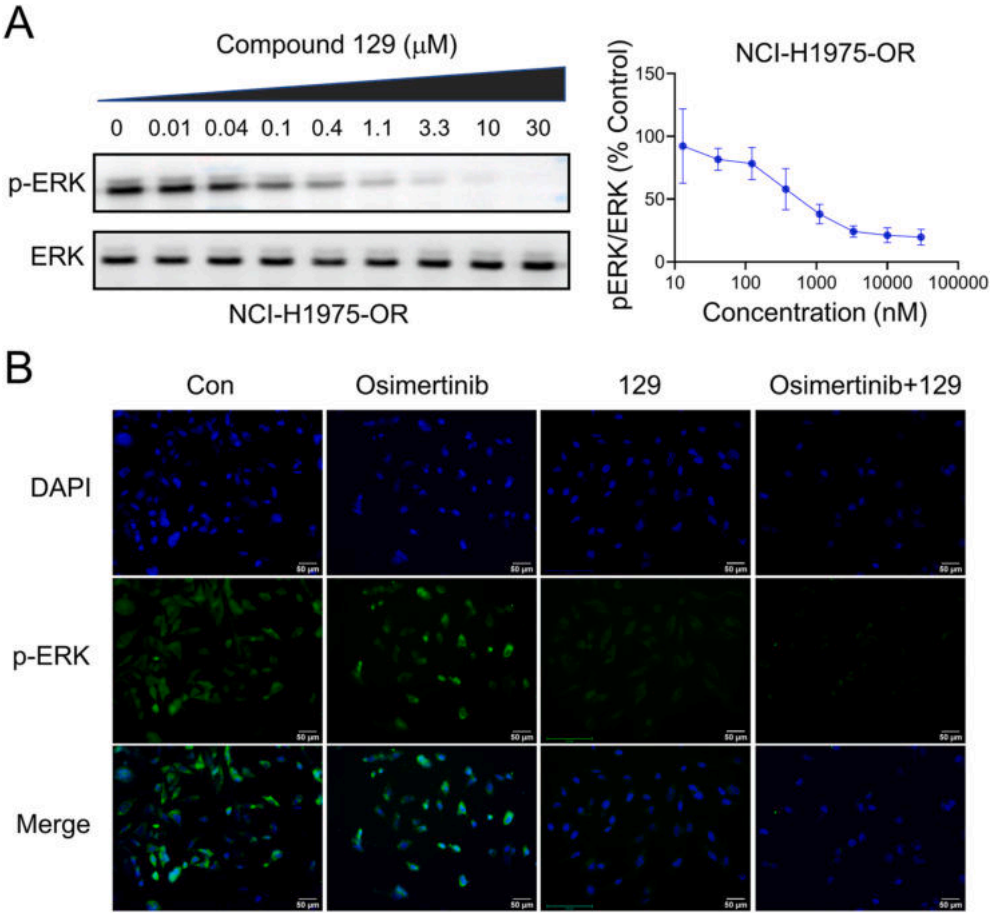

Fig. 5. Compound 129 inhibits phosphorylated ERK (pERK) levels in receptor tyrosine kinase (RTK)-resistant NSCLC cells. (A) p-ERK activity inhibition by increasing the concentration of compound 129 in NCI–H1975-OR cells, assayed by western blotting. (B) H1975 cells treated with osimertinib, 129, or both were stained with DAPI and p-ERK antibodies.

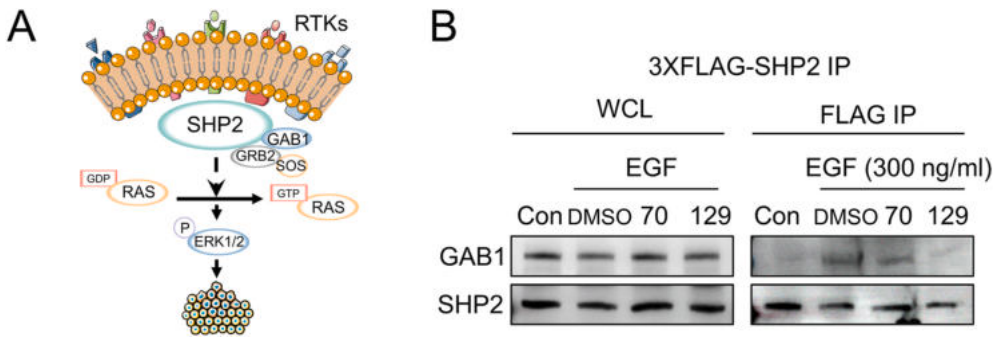

Fig. 6. Compound 129 inhibit SHP2 downsream signalling via disrupting SHP2 related protein association. (A) Schematic illustrate of SHP2 function as the universal transducer of RTKs signalling. (B) The effect of compound 129 on the SHP2-GAB1 association in HEK293T cells. Cells were treated with compound 129 for 1 h (10 μM) and stimulated with 300 ng/ml EGF for 3 min followed by immunoprecipitation of 3 × FLAG–SHP2 by the anti-FLAG beads.

2.9. Selectivity profile of 129 against PTPs and RTKs

Owing to the highly conserved PTPs catalytic domain, it is challenging to discover selective SHP2 inhibitors among PTPs [25]. To investigate the specificity of compound 129, the inhibitory activities were profiled among a panel of mammalian PTPs of different types, including two classical non-receptor PTPs (PTPN1 and PTPN12), a classical receptor type PTP (PTPRA), a VH1-like PTP (PRL2), and a class II PTP named ACP1 (LMW-PTP). As shown in Fig. 7A, 129 showed no measurable activity against the other tyrosine phosphatases. The high level of target selectivity of 129 is likely due to the unique tunnel drug-binding site of SHP2 among the entire PTP family.

The 2,4,5-substituted pyrimidine core is often developed as a kinase inhibitor, especially as a kinase inhibitor such as Syk and Lyk2 inhibitors [26,27]. In this study, compound 129 was prioritized for additional profiling against a panel of 97 kinases (Fig. 7B and Table S3). This screening result revealed compound 129 had no obvious inhibitory effect on all the tested human protein kinases at a concentration of 1000 nM, with only a slight inhibitory effect on LKB1 and PIK3C2B (>35% percent control).

2.10. In vivo pharmacokinetics properties

Compound 129 is a selective SHP2 inhibitor candidate at the molecular and cellular levels. Therefore, in our next study, we explored the pharmacokinetic properties of 129 *in vivo*. Compound 129 was administered IV/PO at 5 mg/kg to male SD rats in a crossover study design. As shown in Table 3, compound 129 demonstrated high clearance, a high volume of distribution (13.9 L/kg), a moderate half-life ($T_{1/2}$ = 5.31 h), as well as good oral bioavailability (F = 55.07 ± 7.93%). Previous pharmacokinetic studies in mice for SHP099 showed good oral exposure and acceptable bioavailability (F = 46%). These results suggest compound 129 has a higher oral bioavailability than SHP099 and is suitable for further *in vivo* anti-tumor evaluation.

2.11. Antitumour efficacy of compound 129 in acute myeloid leukemia xenograft

On the basis of the potent RTK-signalling inhibition effect of compound 129 and its promising pharmacokinetic properties, we next assessed the efficacy of compound 129 in acute myeloid leukemia (AML) model *in vivo*. Anti-leukaemic efficacy was evaluated in a systemic murine NSG xenograft model inoculated with FLT3-ITD mutated MV-4-11-luciferase (MV-4-11-Luc) AML cells. Engrafted mice were treated with vehicle, or compound 129 20 mg/kg dosed daily (Fig. 8A). For comparison, a parallel group of MV-4-11-bearing mice were treated with SHP2 inhibitor SHP099 as positive control. Leukemia cells growth were visualized by bioluminescent imaging. As shown in Fig. 8B and C, compound 129 treatment caused significant reduction of leukemia burden in AML model. At day 28, blood, bone marrow, and splenic tissues of NSG mice were harvested for leukemia cells analysis. The percentage of MV-4-11-Luc cells was quantified via flow cytometric analysis of murine peripheral blood evaluated by anti-human CD45 (hCD45). Administration with 20 mg/kg compound 129 resulted in remarked decreased leukemia burden in mice. Notably, compound 129 treatment near completely eradicated human (h)$CD45^+$ leukaemic cells in blood and spleen (Fig. D). Thus, the pharmacological modulation of SHP2 by 129 is effective *in vivo* and offers a candidate therapeutic agent

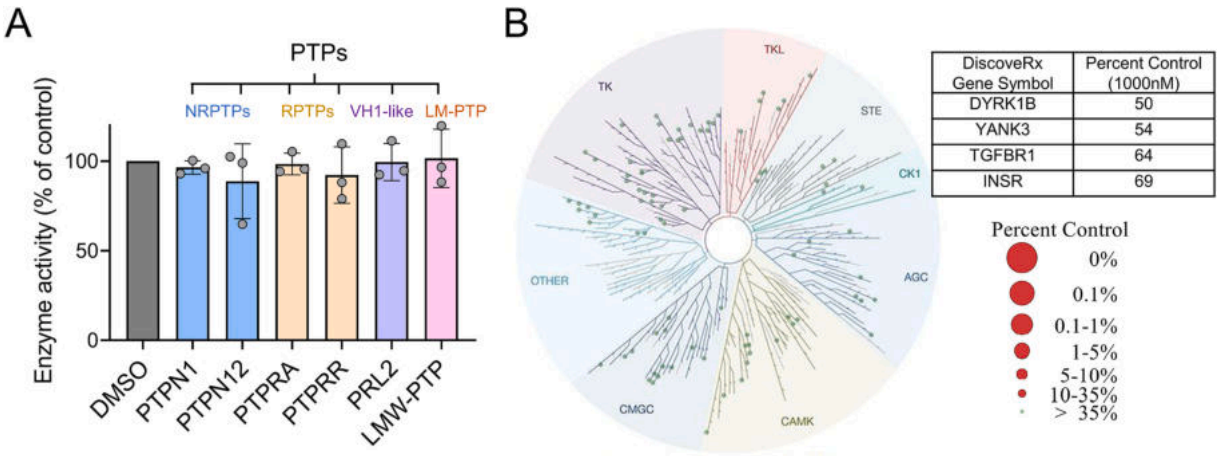

Fig. 7. Selectivity profile of compound 129 against protein tyrosine phosphatases (PTPs) and receptor tyrosine kinases (RTKs). (A) Inhibitory activities of compound 129 against representive mammalian PTPs from different subfamily at 10 μM. (B) Selectivity profile of compound 129 against a 97 kinase panel (scanEDGE).

Table 3
In vivo pharmacokinetic properties of compound 129.

Parameter	$T_{1/2}$	T_{max}	C_{max}	$AUC_{(0-\infty)}$	V_{ss}	CL	F
Unit	h	h	ng/mL	h*ng/mL	mL/kg	mL/h/kg	%
iv (5 mg/kg)	5.31 ± 0.51	0.083 ± 0.01	854.36 ± 129.58	1878.21 ± 220.89	13976.69 ± 835.88	2685.55 ± 299.07	/
po (5 mg/kg)	4.77 ± 0.55	2.17 ± 1.76	101.30 ± 22.33	1038.96 ± 155.49	/	/	55.07 ± 7.93

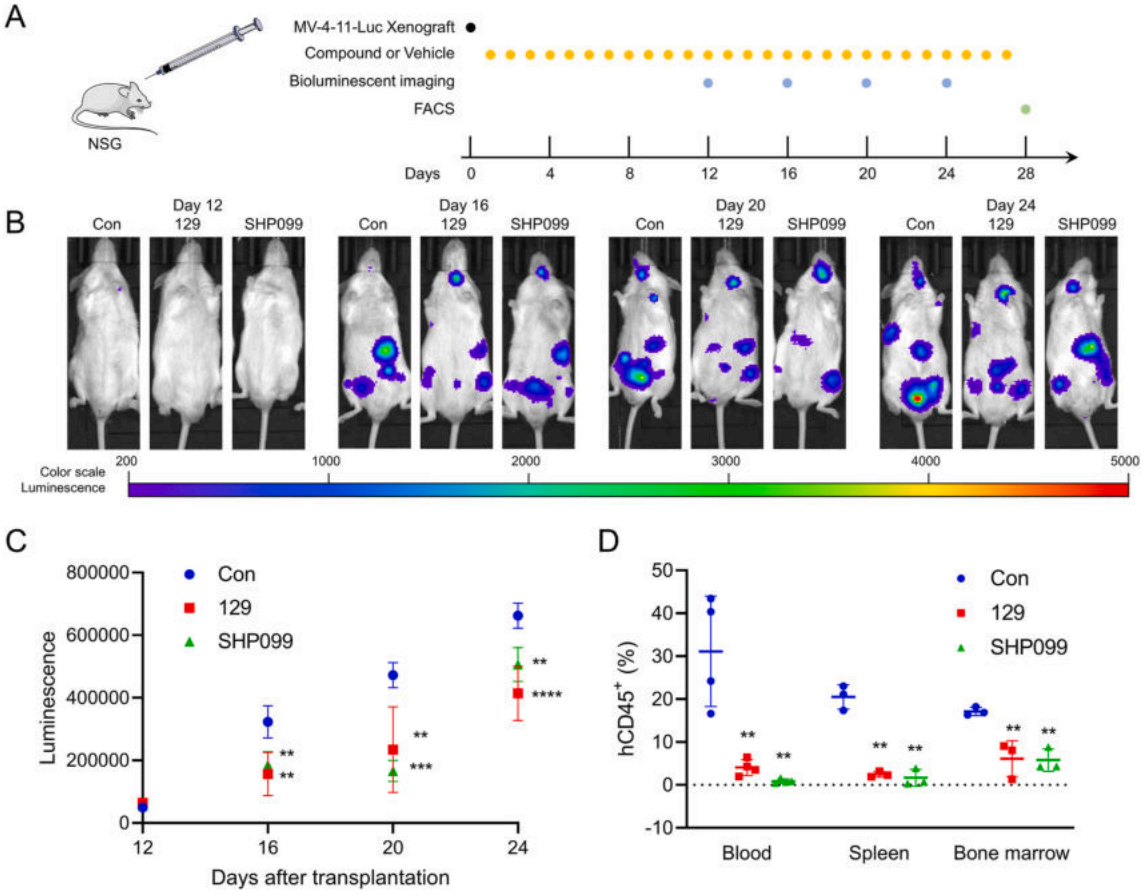

Fig. 8. Antitumour efficacy of compound 129 in AML xenograft. (A) Experimental scheme for xenograft experiments. Blue dots indicate assessment of human MV-4-11-Luc by bioluminescent imaging, orange dots indicate days of compound 129, SHP099, or vehicle (20 mg/kg daily) by oral gavage and green dot denotes terminal analysis on day 28. (B) Representative bioluminescent image of NSG mice that were injected with MV-4-11-Luc cells and treated with either compound 129, SHP099, or vehicle. (C) Qualification of images in (B), n = 5. (D) Tumour burden in the blood, bone marrow and spleen was analyszed by FACS of $hCD45^+$ leukaemic cells at day 28. Bars represent mean ± SD, n = 3–4. Statistical differences between treatment groups were determined using a two-sided Wilcox test with Holm–Bonferroni correction for multiple comparisons.

or lead compound for the treatment of RTK-dependent cancers.

3. Discussion and conclusions

The cooperation between PTPs and RTKs mediates the balance of tyrosine phosphorylation levels. PTPs are key regulators of a wide range of diseases [7,28]. Compared with the rapid development of TKIs, drug discovery for PTPs remains challenging. SHP2 (PTPN11) is a unique member of the PTP family and a suitable drug target for cancer therapy [29–31]. Given its key functional role, the drug development targeting SHP2 is crucial. Due to the polar surface of the catalytic site, SHP2 orthostatic inhibitor development remains challenging. However, SHP2 allosteric inhibitors are among the small molecules currently entering clinical research. To date, eight SHP099 derivatives (e.g. TNO155, RMC-4630, JAB-3068, and RLY-1971) have entered into clinical trials as mono- or combined therapy for treating different cancers [8,14,15]. Several clinical trials of TNO155 in combination with other inhibitors such as nazartinib, eabrafenib, ribociclib, trametinib, naporafenib, or MRTX849 have been undergoing to evaluate the anticancer efficacy. In addition, RMC-4630 in combination with AMG510 (a $KRAS^{G12}C$ inhibitor) has been advanced into a phase II clinical trial for the patients carrying the $KRAS^{G12C}$ mutation [32].

Multiple potential allosteric binding sites of SHP2 have been recognized (e.g., tunnels, latches, and grooves) [13]. The first tunnel site allosteric inhibitor SHP836 was identified by HTS from 100,000-compound libraries, which led to the identification of the improved analogs, SHP099 and TNO155 [14]. The first latch-binding site inhibitor, SHP244 [13], works as a distinct allosteric inhibitor found in 1.5-million compound libraries. Indeed, several major issues remain regarding the identification of SHP2 allosteric inhibitor hits. For instance, a large number of compound libraries are required, and multiple rounds of SHP2 enzyme variants are screened to filter undesired inhibitors. In addition, further co-crystallographic studies are essential to resolve the allosteric binding sites of inhibitors. Only a few allosteric inhibitors are currently in the early clinical stage. Thus, the development of a straightforward screening strategy for the identification of SHP2

allosteric inhibitors and discovery of lead compounds with novel scaffolds is of importance to many scientists.

SBVS has the following advantages over experimental HTS: (1) Improved economical technique to discover hits by screening large virtual compound libraries through *in silico* approaches rather than actual experiments. (2) The speed-enhanced SBVS workflow can significantly shorten the hit identification cycle. (3) The SBVS can achieve higher hit rates [16,17]. Here, a multistep SBVS approach was used to predict potential hits. According to previous studies, tunnel site inhibitors show greater inhibitory potency than latch sites [13]. Therefore, in this study, we prioritized performing an SBVS at the tunnel site. Multiple-step filtering led to the identification of compound 70 with a novel pyrimidine-5-carboxamide core, which was distinct from the common pyrazin core of SHP099, TNO155, and RMC-4630. Systematic structure–based optimization of compound 70 and SAR analysis have resulted in the discovery of a potent inhibitor 129.

Cell-based immunoprecipitation data revealed that compound 129 treatment diminished SHP2's binding to the downstream scaffolding protein GAB1. Thus, compound 129 could disrupt the formation of the signalosome complex that is assembled at RTKs and located at the cell membrane, thereby interfering with RAS–GTP levels in cells [33,34]. Next, we observed compound 129 efficiently inhibited RAS/MAPK signaling in multiple RTK-driven cancers. Notably, 129 exhibited pERK inhibitory effects comparable to those of osimertinib and quizartinib in EGFR and FLT3 driven cancer cells, respectively. Furthermore, compound 129 exhibited similar pERK IC_{50} in H1975 and H1975-OR cells, proving the therapeutic potential of compound 129 in combating the drug resistance of osimertinib. The two major resistance mechanisms of osimertinib are the C797S resistance mutation within the kinase domain and bypass activation of other RTKs, such as FGFR and ALK [22,32,35]. However, RTK-mutated cells still rely on SHP2 for MAPK signal transduction. Furthermore, this also proved that the combined use of the SHP2 inhibitor 129 with osimertinib displayed synergistic effects and could maximize tumor signaling inhibition, which might be a new treatment strategy. Indeed, early clinical trials of the SHP2 inhibitor TNO155 in combination with the EGFR inhibitor nazartinib are underway (phase I, NCT03114319). *In vivo*, compound 129 exhibited promising pharmacokinetic properties and significantly inhibited RTK activated AML cells *in vivo*.

In summary, using a SBVS method targeting SHP2 "tunnel site", we efficiently identified a novel hit compound (70) as the SHP2 allosteric inhibitor. Structure-based chemical modification from compound 70 derived a new and selective inhibitor compound 129. Active compound 129 serves as a new chemical tool for studying of SHP2 function both *in vitro* and *in vivo*. Our study offers a straightforward method for the identification of SHP2 allosteric inhibitors, as well as a valuable candidate for RTK-drinven disease treatment. In addition to cancer, a relationship between SHP2 and other inflammatory or immune diseases has also been reported [28,36,37]. Therefore, the therapeutic effect of candidate compound 129 in SHP2-related models, such as type 2 diabetes, should be evaluated in the future.

4. Experimental section

4.1. Chemistry

In general, commercial reagents including solvents, and other chemicals were used without further purification. Reagents were obtanied from Sigma-Aldrich, Aladdin, and Energy Chemical. All reactions were monitored by TLC. The compounds 1–111, and 113–117 were obtained from the commercial vendors of ChemDiv (Tables S1–2) and the compounds 112, and 118–131 were synthesized (Scheme 1 and Table 2). ^{1}H NMR and ^{13}C NMR spectra were determined on a Bruker 500 MHz instrument. Electronspray ionization mass spectra in positive mode (ESI-MS) results were collected on Waters Alliance (e2695) equipped with QDa and PDA detector (2998). Chromatographic purification was done on Silica Gel 60. The purities of all the synthesized compounds were >95% determined using the analytical HPLC on Shimadzu LC-20AD system equipped with a UV detector (SPD-20A) fitted with a Diamonsil C18 column (5 μm, 250 mm × 4.6 mm). The HPLC traces for all the synthesized compounds are shown in Supporting Information. HRMS were performed on an Agilent Technologies 6546-LC/Q-TOF LC/MS apparatus (ESI-TOF). The HRMS, ^{1}H NMR and ^{13}C NMR spectra data of the synthesized compounds are shown in Supporting Information.

***Ethyl 4-amino-2-(4-((tert-butoxycarbonyl)amino)-4-methylpiperidin-1-yl)pyrimidine-5-carboxylate* (a3).** $Pd_2(dba)_3$ (228.9 mg, 0.25 mmol), Ph_3P(131.1 mg, 0.5 mmol), Sodium *tert*-butoxide (1.44 g, 15 mmol), and 1,4-dioxane (10 mL) were added to a 50 mL two-necked flask. The mixture was sparged with nitrogen and then stirred for 15min. Next, *tert*-butyl (4-methylpiperidin-4-yl)carbamate (**a1**) (504.1 mg, 2.5 mmol) in 1,4-dioxane (7 mL), and ethyl 4-amino-2-chloropyrimidine-5-carboxylate (**a2**, 642.9 mg, 3 mmol) in 1,4-dioxane (7 mL) were added to the flask by syringe and the flask was capped with flap plug. The reaction mixture was stirred at 100 °C for 18 h. After cooling to room temperature, the mixture was diluted with 20 mL EA and washed with sodium bicarbonate saturated solution. The reaction mixture was extracted with EA and concentrated under reduced pressure to give a crude product which was further purified by chromatography on silica gel to give compound **a3** as clear colloidal liquid (701 mg, 74%). ^{1}H NMR (500 MHz, $CDCl_3$) δ 8.59 (s, 1H), 7.62 (s, 1H), 5.45 (s, 1H), 4.55 (s, 1H), 4.27–4.13 (m, 4H), 3.43–3.34 (m, 2H), 2.02–1.95 (m, 2H), 1.55–1.46 (m, 2H), 1.40 (s, 9H), 1.33 (s, 3H), 1.30 (t, J = 7.1 Hz, 3H).

***ethyl 4-amino-2-(4-amino-4-methylpiperidin-1-yl)pyrimidine-5-carboxylate* (a4).** Ethyl 4-amino-2-(4-((tert-butoxycarbonyl)amino)-4-methylpiperidin-1-yl)pyrimidine-5-carboxylate (**a3**) (113.8 mg, 0.3

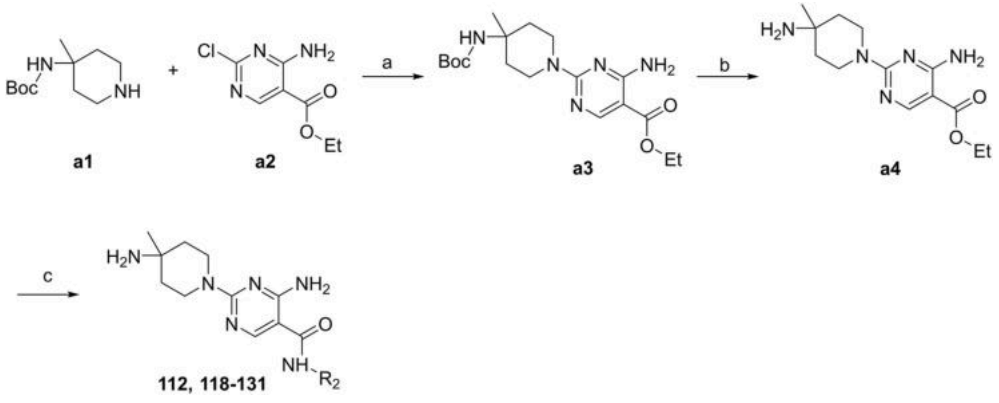

Scheme 1. Reagent and conditions: (a)$Pd_2(dba)_3$, Ph_3P, NaOtBu, dioxane, N_2, 18 h; (b) TFA, DCM, rt, 2 h; (c) R_2NH_2, LiHMDS 2 eq, rt, toluene, N_2, 15 h.

mmol), and DCM (1 mL) were added to a 25 mL two-necked flask. A solution of 25% TFA in dichloromethane (6 mL) was added dropwise with syringe at 0 °C. The mixture was stirred at room temperature for 3 h. The mixture was alkalinized to pH 10 with saturated Na_2CO_3 solution, extracted with EA and concentrated under reduced pressure to give a crude product which was purified by chromatography on silica gel to give the compound **a4** in 82% yield (70 mg). ^{1}H NMR (500 MHz, $CDCl_3$) δ 8.62 (s, 1H), 7.65 (br s, 1H), 5.21 (br s, 1H), 4.27 (q, 2H), 4.01 − 3.88 (m, 2H), 3.85 − 3.70 (m, 2H), 1.76 (s, 4H), 1.68 − 1.52 (m, 3H), 1.51 − 1.43 (m, 2H), 1.34 (t, J = 7.1 Hz,3H).

***General Procedure for the Synthesis of target compound 112, and 118–131. Exemplified by 4-amino-2-(4-amino-4-methylpiperidin-1-yl)-N-phenylpyrimidine-5-carboxamide* (112).** Ethyl 4-amino-2-(4-amino-4-methylpiperidin-1-yl)pyrimidine-5-carboxylate (**a4**) (27.9 mg, 0.1 mmol) was dissolved in 1 mL of toluene in a pressure-proof pipe under nitrogen. Aniline (0.3 mmol) and LiHMDS (0.3 mL, 0.3 mmol) were added to the mixture sequentially. The reaction mixture was stirred at room temperature for 15 h. The mixture was quenched with 1 M NH_4Cl solution and filtered through silica gel powder. Then, the reaction mixture was eluted with ethyl acetate (3 × 1 mL) and concentrated under reduced pressure to afford the crude product, which was purified by chromatography on silica gel to give the target product in 95% yield (31 mg). ^{1}H NMR (500 MHz, DMSO-d_6) δ 10.06 (s, 1H, NHCO), 8.72 (s, 1H, pyrimidine-H), 7.73–7.67 (m, 2H, Ar–H), 7.34–7.27 (m, 2H, Ar–H), 7.09–7.02 (m, 1H, Ar–H), 4.29–4.20 (m, 2H, piperidine-H), 3.55–3.46 (m, 2H, piperidine-H), 1.83–1.63 (m, 4H, piperidine-H), 1.39 (s, 3H, –CH_3). ^{13}C NMR (101 MHz, DMSO-d_6) δ 166.1, 163.4, 161.0, 158.4, 139.6, 128.9, 123.6, 121.0, 99.2, 52.6, 40.5, 40.3, 40.0, 39.8, 39.6, 39.4, 39.2, 34.9, 22.7. LC-MS (ESI$^+$): calcd for $C_{17}H_{23}N_6O$ = 327.19, found; [M + H]$^+$ = 327.36. HRMS(ESI): calcd for $C_{17}H_{23}N_6O$ [M + H]$^+$, 327.1933; found, 327.1932.

***4-amino-2-(4-amino-4-methylpiperidin-1-yl)-N-(naphthalen-1-yl) pyrimidine-5-carboxamide (118)*.** ^{1}H NMR (500 MHz, DMSO-d_6) δ 10.08 (s, 1H, NHCO), 8.84 (s, 1H, pyrimidine-H), 7.99–7.91 (m, 2H, Ar–H), 7.83 (dd, J = 6.7, 2.8 Hz, 1H, Ar–H), 7.57–7.49 (m, 4H,Ar–H), 4.07 (dd, J = 13.4, 6.4 Hz, 2H, piperidine-H), 3.73–3.62 (m, 2H,piperidine-H), 1.67–1.52 (m, 4H, piperidine-H), 1.28 (s, 3H, –CH_3). ^{13}C NMR (101 MHz, DMSO-d_6) δ 167.0, 163.5, 161.2, 158.4, 134.3, 134.2, 129.9, 128.4, 126.5, 126.4, 126.3, 125.9, 124.5, 123.9, 98.6, 50.9, 40.5, 40.3, 40.1, 39.9, 39.7, 39.5, 39.3, 36.4, 25.3, 23.4. LC-MS (ESI$^+$): calcd for $C_{21}H_{25}N_6O$ = 377.20, found; [M + H]$^+$ = 377.29. HRMS(ESI): calcd for $C_{21}H_{25}N_6O$ [M + H]$^+$, 377.2090; found, 377.2088.

***4-amino-2-(4-amino-4-methylpiperidin-1-yl)-N-(naphthalen-2-yl) pyrimidine-5-carboxamide (119)*.** ^{1}H NMR (500 MHz, DMSO-d_6) δ 10.11 (s, 1H, NHCO), 8.71 (s, 1H, pyrimidine-H), 8.31 (d, J = 2.0 Hz, 1H, Ar–H), 7.89–7.79 (m, 3H,Ar–H), 7.76 (dd, J = 8.9, 2.1 Hz, 1H, Ar–H), 7.63–7.57 (m, 1H, Ar–H), 7.51–7.44 (m, 1H, Ar–H), 4.13–4.06 (m, 2H, piperidine-H), 3.69–3.60 (m, 2H, piperidine-H), 1.67–1.55 (m, 4H, piperidine-H), 1.30 (s, 3H, –CH_3). ^{13}C NMR (101 MHz, DMSO-d_6) δ 166.3, 163.4, 161.1, 158.4, 137.3, 133.8, 130.2, 128.4, 127.9, 127.7, 126.7, 125.0, 121.7, 116.9, 99.2, 51.9, 40.6, 40.5, 40.4, 40.3, 40.2, 40.1, 39.9, 39.7, 39.5, 39.3, 35.5, 23.7. LC-MS (ESI$^+$): calcd for $C_{21}H_{25}N_6O$ = 377.20, found; [M + H]$^+$ = 377.29. HRMS(ESI): calcd for $C_{21}H_{25}N_6O$ [M + H]$^+$, 377.2090; found, 377.2082.

***N-([1,1′-biphenyl]-3-yl)-4-amino-2-(4-amino-4-methylpiperidin-1-yl)pyrimidine-5-carboxamide (120)*.** ^{1}H NMR (500 MHz, DMSO-d_6) δ 9.95 (s, 1H, NHCO), 8.66 (s, 1H, pyrimidine-H), 7.99 (t, J = 2.0 Hz, 1H, Ar–H), 7.72–7.66 (m, 1H, Ar–H), 7.66–7.61 (m, 2H, Ar–H), 7.48 (t, J = 7.7 Hz, 2H, Ar–H), 7.44–7.32 (m, 3H, Ar–H), 3.86–3.79 (m, 4H, piperidine-H), 1.47 (t, J = 5.8 Hz, 4H, piperidine-H), 1.16 (s, 3H, –CH_3). ^{13}C NMR (101 MHz, DMSO-d_6) δ 166.2, 163.4, 161.1, 158.3, 140.9, 140.6, 140.2, 129.6, 129.4, 128.0, 127.0, 122.0, 119.8, 119.1, 98.8, 49.1, 40.5, 40.4, 40.3, 40.2, 40.1, 39.9, 39.7, 39.5, 39.3, 38.2. LC-MS (ESI$^+$): calcd for $C_{23}H_{27}N_6O$ = 403.22, found; [M + H]$^+$ = 403.36. HRMS(ESI): calcd for $C_{23}H_{27}N_6O$ [M + H]$^+$, 403.2246; found, 403.2249.

***4-amino-2-(4-amino-4-methylpiperidin-1-yl)-N-(9H-fluoren-2-yl) pyrimidine-5-carboxamide (121)*.** ^{1}H NMR (500 MHz, DMSO-d_6) δ 9.96 (s, 1H, NHCO), 8.65 (s, 1H, pyrimidine-H), 7.97 (d, J = 1.9 Hz, 1H, Ar–H), 7.85–7.80 (m, 2H, Ar–H), 7.64 (dd, J = 8.3, 1.9 Hz, 1H, Ar–H), 7.56 (d, J = 7.5 Hz, 1H, Ar–H), 7.39–7.33 (m, 1H, Ar–H), 7.30–7.23 (m, 1H, Ar–H), 4.06–3.97 (m, 2H, piperidine-H), 3.91 (s, 2H, –CH_2-), 3.73–3.65 (m, 2H, piperidine-H), 1.56 (t, J = 5.8 Hz, 4H, piperidine-H), 1.25 (s, 3H, –CH_3). ^{13}C NMR (101 MHz, DMSO-d_6) δ 166.1, 163.4, 161.1, 158.2, 143.9, 143.2, 141.5, 138.7, 136.8, 127.2, 126.5, 125.4, 120.3, 119.9, 119.7, 117.7, 99.2, 50.9, 40.5, 40.3, 40.1, 39.9, 39.7, 39.5, 39.2, 36.9, 36.4, 25.3, 24.0. LC-MS (ESI$^+$): calcd for $C_{24}H_{27}N_6O$ = 415.22, found; [M + H]$^+$ = 415.22. HRMS(ESI): calcd for $C_{24}H_{27}N_6O$ [M + H]$^+$, 415.2246; found, 415.2239.

***4-amino-2-(4-amino-4-methylpiperidin-1-yl)-N-(4-methoxyphenyl)pyrimidine-5-carboxamide (122)*.** ^{1}H NMR (500 MHz, DMSO-d_6) δ 9.78 (s, 1H, NHCO), 8.61 (s, 1H, pyrimidine-H), 7.58–7.51 (m, 2H, Ar–H), 6.92–6.86 (m, 2H, Ar–H), 4.07–3.99 (m, 2H, piperidine-H), 3.73 (s, 3H, -OCH_3), 3.68–3.60 (m, 2H, piperidine-H), 1.62–1.52 (m, 4H, piperidine-H), 1.26 (s, 3H, –CH_3). ^{13}C NMR (101 MHz, DMSO-d_6) δ 165.8, 163.4, 161.1, 158.0, 155.7, 132.5, 122.7, 114.0, 99.1, 55.6, 51.1, 40.5, 40.3, 40.1, 39.9, 39.7, 39.58, 39.50, 39.2, 36.2, 24.8, 23.7. LC-MS (ESI$^+$): calcd for $C_{18}H_{25}N_6O_2$ = 357.20, found; [M + H]$^+$ = 357.23. HRMS(ESI): calcd for $C_{18}H_{25}N_6O_2$ [M + H]$^+$, 357.2039; found, 357.2037.

***4-amino-2-(4-amino-4-methylpiperidin-1-yl)-N-(3,4-dimethoxyphenyl)pyrimidine-5-carboxamide (123)*.** ^{1}H NMR (500 MHz, DMSO-d_6) δ 9.77 (s, 1H, NHCO), 8.61 (s, 1H, pyrimidine-H), 7.34 (d, J = 2.4 Hz, 1H, Ar–H), 7.20 (dd, J = 8.7, 2.4 Hz, 1H, Ar–H), 6.90 (d, J = 8.8 Hz, 1H, Ar–H), 4.25 (d, J = 13.1 Hz, 2H, piperidine-H), 3.73 (d, J = 4.3 Hz, 6H,-OCH_3),3.50–3.43 (m, 2H, piperidine-H), 1.68 (t, J = 4.9 Hz, 4H, piperidine-H), 1.37 (s, 3H,-CH_3). ^{13}C NMR (101 MHz, DMSO-d_6) δ 165.7, 163.3, 161.0, 158.0, 148.7, 145.3, 133.0, 112.9, 112.2, 106.2, 99.4, 56.1, 55.8, 52.5, 40.5, 40.3, 40.1, 39.9, 39.7, 39.5, 39.3, 34.9, 22.7. LC-MS (ESI$^+$): calcd for $C_{19}H_{27}N_6O_3$ = 387.21, found; [M + H]$^+$ = 387.29. HRMS(ESI): calcd for $C_{19}H_{27}N_6O_3$ [M + H]$^+$, 387.2145; found, 387.2137.

***4-amino-2-(4-amino-4-methylpiperidin-1-yl)-N-(2,6-dimethoxyphenyl)pyrimidine-5-carboxamide (124)*.** ^{1}H NMR (500 MHz, DMSO-d_6) δ 8.99 (s, 1H, NHCO), 8.66 (s, 1H, pyrimidine-H), 7.23 (t, J = 8.4 Hz, 1H, Ar–H), 6.70 (d, J = 8.5 Hz, 2H, Ar–H), 4.24–4.16 (m, 2H, piperidine-H), 3.73 (s, 6H, -OCH_3), 3.60–3.45 (m, 2H, piperidine-H), 1.66 (q, J = 5.1, 4.6 Hz, 4H, piperidine-H), 1.35 (s, 3H, –CH_3). ^{13}C NMR (101 MHz, DMSO-d_6) δ 166.1, 163.5, 161.2, 156.7, 115.0, 104.7, 99.0, 56.1, 52.6, 40.5, 40.3, 40.1, 39.9, 39.7, 39.5, 39.3, 34.9, 22.7. LC-MS (ESI$^+$): calcd for $C_{19}H_{27}N_6O_3$ = 387.21, found; [M + H]$^+$ = 387.29. HRMS(ESI): calcd for $C_{19}H_{27}N_6O_3$ [M + H]$^+$, 387.2145; found, 387.2133.

***4-amino-2-(4-amino-4-methylpiperidin-1-yl)-N-(4-nitrophenyl) pyrimidine-5-carboxamide (125)*.** ^{1}H NMR (500 MHz, DMSO-d_6) δ 10.41 (brs, 1H, NHCO), 8.68 (s, 1H, pyrimidine-H), 8.26–8.19 (m, 2H, Ar–H), 7.99–7.92 (m, 2H, Ar–H), 7.56 (brs, 2H, pyrimidine-NH_2), 3.95–3.77 (m, 4H, piperidine-H), 1.50 (t, J = 5.8 Hz, 4H, piperidine-H), 1.19 (s, 3H, –CH_3). ^{13}C NMR (101 MHz, DMSO-d_6) δ 166.6, 163.4, 161.1, 159.0, 146.3, 142.3, 125.2, 120.0, 98.4, 50.0, 40.5, 40.3, 40.1, 39.9, 39.7, 39.52 39.3, 37.3, 26.9. LC-MS (ESI$^+$): calcd for $C_{17}H_{22}N_7O_3$ = 372.17, found; [M + H]$^+$ = 372.23. HRMS(ESI): calcd for $C_{17}H_{22}N_7O_3$ [M + H]$^+$, 372.1784; found, 372.1780.

***4-amino-2-(4-amino-4-methylpiperidin-1-yl)-N-(4-fluorophenyl) pyrimidine-5-carboxamide (126)*.** ^{1}H NMR (500 MHz, DMSO-d_6) δ 9.91 (s, 1H, NHCO), 8.61 (s, 1H, pyrimidine-H), 7.70–7.62 (m, 2H, Ar–H), 7.51 (brs, 2H, Pyrimidine-NH_2), 7.20–7.11 (m, 2H, Ar–H), 3.95–3.86 (m, 2H, piperidine-H), 3.76 (dt, J = 11.7, 5.0 Hz, 2H, piperidine-H), 1.50 (t, J = 5.8 Hz, 4H, piperidine-H), 1.20 (s, 3H, –CH_3). ^{13}C NMR (101 MHz, DMSO-d_6) δ 166.0, 163.3, 161.1, 158.2, 157.3, 135.94, 135.91, 122.8, 122.7, 115.6, 115.4, 98.8, 50.4, 40.5, 40.3, 40.1, 39.9, 39.7, 39.5, 39.3, 37.0, 26.3. LC-MS (ESI$^+$): calcd for $C_{17}H_{22}FN_6O$ = 345.18, found; [M + H]$^+$ = 345.36. HRMS(ESI): calcd for $C_{17}H_{22}FN_6O$ [M + H]$^+$, 345.1839;

found, 345.1837.

4-amino-2-(4-amino-4-methylpiperidin*-1-yl*)-N-(3,4-dichlorophenyl)pyrimidine-5-carboxamide (127). ^{1}H NMR (500 MHz, DMSO-d_6) δ 10.05 (s, 1H, NHCO), 8.60 (s, 1H, pyrimidine-H), 8.04 (d, J = 2.4 Hz, 1H, Ar–H), 7.64 (dd, J = 8.8, 2.4 Hz, 1H, Ar–H), 7.57 (d, J = 8.8 Hz, 1H, Ar–H), 7.50 (brs, 2H, pyrimidine-NH_2), 3.96–3.88 (m, 2H, piperidine-H), 3.77–3.68 (m, 2H, piperidine-H), 1.47–1.36 (m, 4H, piperidine-H), 1.12 (s, 3H, –CH_3). ^{13}C NMR (101 MHz, DMSO-d_6) δ 166.3, 163.3, 161.1, 158.5, 139.9, 131.1, 130.8, 124.8, 121.7, 120.6, 98.3, 48.9, 40.5, 40.4, 40.3, 40.2, 40.1, 39.9, 39.7, 39.5, 39.3, 38.4, 28.8. LC-MS (ESI$^+$): calcd for $C_{17}H_{21}Cl_2N_6O$ = 395.11, found; [M + H]$^+$ = 395.23. HRMS(ESI): calcd for $C_{17}H_{21}Cl_2N_6O$ [M + H]$^+$, 395.1154; found, 395.1148.

4-amino-2-(4-amino-4-methylpiperidin*-1-yl*)-N-(3,5-dichlorophenyl)pyrimidine-5-carboxamide (128). ^{1}H NMR (500 MHz, DMSO-d_6) δ 10.59 (s, 1H, NHCO), 8.83 (s, 1H, pyrimidine-H), 7.93 (d, J = 1.9 Hz, 2H, Ar–H), 7.23 (t, J = 1.9 Hz, 1H, Ar–H), 4.24–4.17 (m, 2H, piperidine-H), 3.49 (s, 2H, piperidine-H), 1.78–1.62 (m, 4H, piperidine-H), 1.36 (s, 3H, –CH_3). ^{13}C NMR (101 MHz, DMSO-d_6) δ 166.5, 163.3, 161.1, 158.9, 142.3, 134.1, 122.5, 118.7, 98.6, 52.4, 40.5, 40.3, 40.1, 39.9, 39.6, 39.4, 39.2, 35.1, 23.0. LC-MS (ESI$^+$): calcd for $C_{17}H_{21}Cl_2N_6O$ = 395.11, found; [M + H]$^+$ = 395.29. HRMS(ESI): calcd for $C_{17}H_{21}Cl_2N_6O$ [M + H]$^+$, 395.1154; found, 395.1146.

4-amino-2-(4-amino-4-methylpiperidin*-1-yl*)-N-(pyridin*-3-yl*)pyrimidine-5-carboxamide (129). ^{1}H NMR (500 MHz, DMSO-d_6) δ 10.07 (s, 1H, NHCO), 8.83 (d, J = 2.6 Hz, 1H, pyridine-H), 8.67 (s, 1H, pyrimidine-H), 8.26 (dd, J = 4.7, 1.5 Hz, 1H, pyridine-H), 8.07 (dt, J = 8.3, 2.1 Hz, 1H, pyridine-H), 7.35 (dd, J = 8.4, 4.7 Hz, 1H, pyridine-H), 3.91–3.76 (m, 4H, piperidine-H), 1.49 (t, J = 5.7 Hz, 4H, piperidine-H), 1.18 (s, 3H, –CH_3). ^{13}C NMR (101 MHz, DMSO-d_6) δ 166.4, 163.3, 161.1, 158.6, 144.5, 142.6, 136.3, 127.9, 123.8, 98.7, 98.7, 52.5, 40.5, 40.3, 40.1, 39.9, 39.7, 39.5, 39.3, 34.9, 22.7. LC-MS (ESI$^+$): calcd for $C_{16}H_{21}N_7ONa$ = 350.18, found; [M + Na]$^+$ = 350.30. HRMS(ESI): calcd for $C_{16}H_{22}N_7O$ [M + H]$^+$, 328.1886; found, 328.1880.

4-amino-2-(4-amino-4-methylpiperidin*-1-yl*)-N-(pyridin-2-ylmethyl)pyrimidine-5-carboxamide (130). ^{1}H NMR (500 MHz, DMSO-d_6) δ 8.81 (t, J = 6.0 Hz, 1H, NHCO), 8.56 (s, 1H, pyrimidine-H), 8.52–8.47 (m, 1H, pyridine-H), 7.78–7.71 (m, 1H, pyridine-H), 7.32–7.22 (m, 2H, pyridine-H), 4.49 (d, J = 5.9 Hz, 2H, HNCH_2), 3.99–3.89 (m, 2H, piperidine-H), 3.72–3.64 (m, 2H, piperidine-H), 1.52 (t, J = 5.8 Hz, 4H, piperidine-H), 1.22 (s, 3H, –CH_3). ^{13}C NMR (101 MHz, DMSO-d_6) δ 167.3, 163.3, 161.1, 159.6, 157.6, 149.2, 137.1, 122.4, 121.2, 98.5, 50.7, 44.5, 40.5, 40.3, 40.3, 40.18, 40.12, 39.9, 39.7, 39.5, 39.2, 36.6, 25.6. LC-MS (ESI$^+$): calcd for $C_{17}H_{23}N_7ONa$ = 364.20, found; [M + Na]$^+$ = 364.29. HRMS(ESI): calcd for $C_{17}H_{24}N_7O$ [M + H]$^+$, 342.2042; found, 342.2041.

4-amino-2-(4-amino-4-methylpiperidin*-1-yl*)-N-(pyridin*-2-yl*)pyrimidine-5-carboxamide (131). ^{1}H NMR (500 MHz, DMSO-d_6) δ 10.38 (brs, 1H, NHCO), 8.69 (s, 1H, pyrimidine-H), 8.37–8.32 (m, 1H, pyridine-H), 8.04–7.98 (m, 1H, pyridine-H), 7.82–7.75 (m, 1H, pyridine-H), 7.58 (s, 2H, pyrimidine-NH_2), 7.14–7.08 (m, 1H, pyridine-H), 4.01–3.92 (m, 2H, piperidine-H), 3.76–3.68 (m, 2H, piperidine-H), 1.61–1.49 (m, 4H, piperidine-H), 1.24 (s, 3H, –CH_3). ^{13}C NMR (101 MHz, DMSO-d_6) δ 166.6, 163.5, 161.0, 159.0, 152.7, 148.2, 138.3, 119.7, 115.3, 98.5, 51.7, 40.5, 40.3, 40.1, 39.9, 39.7, 39.5, 39.3, 35.7, 24.0. LC-MS (ESI$^+$): calcd for $C_{16}H_{21}N_7ONa$ = 350.18, found; [M + Na]$^+$ = 350.23. HRMS(ESI): calcd for $C_{16}H_{22}N_7O$ [M + H]$^+$, 328.1886; found, 328.1880.

4.2. SBVS of SHP2 tunnel site

The crystal structure of SHP2 used for SBVS was retrieved from the Protein Data Bank (PDB entry:5EHR) [2]. The cascade docking-based SBVS was implemented via the *Virtual Screening Workflow module* in *Schrödinger* software, similar to our previously reported model [18,19]. The top-ranked 5000 molecules were clustered according to two-dimensional (2D) similarity and the resulting clustered 500 molecules were filtered by binding poses. Finally, 97 potential compounds, purchased from the ChemDiv database, were submitted for *in vitro* validation.

4.3. MD simulations and binding free energy estimations

The optimal docked structures of SHP2 bound to compound 70 and 129 were designated as the initial structures for MD simulations. The primary procedures were similar to those in our previous study, including calculation of the compound 70 and 129 partial charges, alignment of force fields to the proteins and ligands, solvation of the systems and addition of counter ions, system minimization, heating, and equilibration [18,19]. Finally, each system was subjected to three parallel 600 ns MD simulations in a constant-temperature, constant-pressure ensemble (NPT) (temperature = 300 K, pressure = 1 bar). The other simulation parameters were set as previously reported [18,19]. Based on a modified MM/GBSA method named VAD-MM/GBSA, as previously reported, MD trajectories of compound 70 and 129 from 500 to 600 ns with 1000 snapshots were applied to the binding free energy estimations and per-residue decomposition [21].

4.4. Protein expression and purification

Bacterial expression constructs of human SHP2 were engineered by cloning the *PTPN11* gene encoding SHP2-FL (Met-1–Leu-525) and SHP2-PTP (Ala-237–Ile-529) into pET30. Site-directed mutations were then introduced using a Q5 mutagenesis kit to obtain SHP2$^{T253M/Q257L}$ and SHP2^{E76K} mutants. The constructs were transformed into competent cells in LB media. SHP2 expression was induced with 1 mM IPTG at 20 °C overnight. Following induction, cell pellets were lysed using a homogenizer (lysis buffer: 50 mM Tris-HCl, 150 mM NaCl, and 50 mM imidazole with 10% glycerol). The collected supernatants were then loaded to a Ni-NTA column and eluted with 200 and 500 mM imidazole buffer. Subsequently, the protein was applied to a HiTrap Q anion exchange column and a size-exclusion chromatography Superdex 200 column. The same protocols were used for the expression and purification of SHP2 mutants. For other PTPs, the catalytic domains of PTPN12, PTP4A2, PTPRR and full-length LMWPTP were subcloned into pET28a and purified in our laboratory. Other PTPs (PTP1B and PTPRA) were obtained from SinoBiological (Beijing, China).

4.5. SHP2 inhibition assay

The dephosphorylation activity of SHP2 was evaluated by the classical phosphatase substrate DiFMUP (Thermo Fisher, #D22065) in a fluorescence assay. The DiFMUP phosphatase assay was tested in a 384-well plate (Griener, #781086). Hit compounds were purchased from ChemDiv and dissolved in DMSO (10 mM stock). SHP2-FL protein (0.5 nM) was co-incubated with 5 μL of the test compounds at various concentrations with 0.5 μM of pIRS-1 peptide added. The pIRS-1 peptide was synthesized by ChinaPeptides (Shanghai) Ltd. with a purity of >97%. After co-incubation for 0.5 h, DiFMUP was added to start the reaction and incubated at r.t. for 30 min. Finally, the reaction stop reagent, bpV (Phen), was supplied to quench the reaction. A plate reader (SpectraMax iD5, Molecular Devices) was used for measurements, with excitation and emission wavelengths at 340 and 450 nm, respectively.

4.6. Cell-based study and western blotting

Human HuH-7 (cat. No. SCSP-526), NCI–H1975 (Cat. No. SCSP-597), NCI–H2228 (Cat. No. SCSP-5001), MV-4-11 (Cat. No. SCSP-5031), and HEK-293T cells (Cat. No. SCSP-502) were purchased from the Cell Bank of the Chinese Academy of Sciences. HuH-7 and MV-4-11 cells were cultured in Dulbecco's modified Eagle's medium (DMEM) (Cat. No. BC-M-005; Bio-Channel) containing 10% FBS (Cat. No. BC-SE-FBS07; Bio-

Channel), and penicillin/streptomycin (cat. No. BL505A; Biosharp). NCI–H1975 and NCI–H2228 cells were cultured in RPMI-1640 (Cat. No. BC-M-017; Bio-Channel) containing 10% FBS, 100 U/ml penicillin, and 100 μg/ml streptomycin.

For western-blot analysis, protein samples were separated by SDS-PAGE, transferred to polyvinylidene difluoride (PVDF) membranes in transfer buffer, and incubated overnight at 4 °C with target antibodies diluted in 5% BSA in phosphate buffered saline Tween (PBST). Enhanced chemiluminescence reagents (NcmECL Ultra; Cat. No. P10300A; NCM Biotech) were used to visualize the antibodies in the Vilber Fusion FX. The following primary antibodies (antigen, dilution, vendor) were used: anti-p-ERK (T202/Y204) (1:2000, Cat. No. #4370), anti-ERK (1:1000; Cat. No. #4695) were purchased from Cell Signaling Technology, anti-Flag (1:5000, Cat. No. 0912-1), anti-GRB2 (1:1000, Cat. No. ER31203), anti-GAB1 (1:1000, Cat. No. ET7106-70), anti-β-actin (1:5000, Cat. No. R1207-1) antibodies, and HRP-conjugated goat anti-rabbit IgG secondary antibodies (1:100000, Cat. No. HA1001) was purchased from HUABIO.

For immunofluorescence analysis, cells were fixed with 2% formaldehyde in PBS for 2 min, permeabilized with 0.5% Triton X-100 in PBS for 10 min and blocked with 5% BSA in PBS for 1 h. Fixed cells were incubated with anti-p-ERK antibody overnight. Following washing thrice with PBS, the cells were stained with Alexa Fluor 488-conjugated secondary antibodies (Cat. No. A0423; Beyotime Biotechnology) for 1 h and DAPI (Cat. No. C1002, Beyotime Biotechnology) for 10 min.

4.7. Clone formation experiment

Clone formation rate was determined using a plate clone formation assay. In total, approximately 200 cells were seeded to each well in a 6-well plate. The wells were then treated with DMSO or the test compound at 37 °C for 14 d, gently washed, and stained with crystal violet.

4.8. Establishment of NCI–H1975-OR cells

Osimertinib-resistant NCI–H1975 cells were established as previous described [38]. NCI–H1975 cells were treated with 30 nM osimertinib for three days. The cells were then grown in drug-free medium until they recovered to a normal growth rate. For the selection cycles, the cells were exposed to gradually increasing concentrations of osimertinib from 30 to 2000 nM. After approximately six months, the H1975 cells were resistant to osimertinib.

4.9. Co-immunoprecipitation

HEK-293T cells were transfected with 3X Flag-SHP2 plasmids by jetPRIME. After transfection, cells were treated with DMSO or the test compound overnight. Following treatment, the cells were treated with recombinant hEGF (Cat. No. P5552; Beyotime Biotechnology) at 300 ng/mL for 3 min. The medium was immediately removed, and co-immunoprecipitation assays were performed using a Flag-tag Protein IP Assay Kit with agarose gel (Cat. No. P2202, Beyotime Biotechnology) following the manufacturer's instructions.

4.10. KINOME profiling

The kinase selectivity profile was tested on Eurofins KINOMEscan platform (https://www.eurofinsdiscoveryservices.com/). Active compounds were screened at a concentration of 1000 nM against 97 targets (scanEDGE). Results of the screening are presented as '% Ctrl', with lower numbers indicating stronger inhibition.

4.11. Pharmacokinetic parameters

The pharmacokinetic parameters of compound 129 were obtained from Shanghai Medicilon Inc. (Medicilon.com). Compound 129 was dissolved in a vehicle of 5% DMSO, 10% Solutol, and 85% of (10% HP-®-CD in saline, PH = 9–10). Male Sprague Dawley (SD) rats were administered compound 129 solution intravenously (i. v.) at 1 mg/kg and by p.o. at 10 mg/kg. At time points of 0.25, 0.5, 1, 2, 4, 6, 8, and 24 h (po) or 0.083, 0.25, 0.5, 1, 2, 4, 8, and 24 h (i.v.) post-treatment, blood samples from each experimental rat were collected and centrifuged. The plasma supernatant samples were analyzed using LC-MS/MS (TQ6500+).

4.12. In vivo tumour xenograft experiments

All animal experiments were conducted in accordance to guidelines approved by the licensing committee of Hangzhou Medical College, P. R. China. Male NOD-SCID IL2Rgamma (NSG) mice (GemPharmatech, China), 6–8 weeks old were transplanted with 1×10^6 MV-4-11-Luc cells via tail vein injections in each mouse. Mice were randomized post xenograft transplantation into cages of five mice. Mice were randomly split into two groups and were given intraperitoneal injections of vehicle, Compound 129 or SHP099 at 20 mg/kg of mice daily. Circulating AML progression was analyzed weekly by bioluminescence imaging using Spectrum Imager. Mice were sacrificed at end of the experiment. Blood, spleen, and bone marrow were isolated as indicated, cells were separated by tissue homogenization and analyzed by flow cytometry.

For analysis of mouse xenografts, red blood cells were lysed with RBC Lysis Buffer at room temperature (Cat. No. 00-4300-54, ThermoFisher), with remaining cells washed and resuspended in Flow Cytometry Staining Buffer (Cat. No. 00-4222-57, ThermoFisher). Blood, spleen and bone marrow cells were stained for 30 min with the following antibodies: human CD45-APC (Cat. No. 555485, BD Bioscience), murine CD45-PE (Cat. No. 103106, BD Bioscience) and Fixable Viability Dye eFluor™ 520 (Cat. No. 65-0867-14, ThermoFisher). Cells were washed and submitted for flow cytometric analysis using BD AccuriTM C6 plus Flow cytometer (BD Bioscience) and Flowjo software (BD Bioscience).

4.13. Statistics and reproducibility

Statistical analyses were performed using GraphPad Prism 8.0 (GraphPad Software). Data are expressed as the mean ± standard error of the mean (SEM). Statistically significant differences between pairs of groups were determined using one-way analysis of variance (ANOVA), whereas those between multiple groups were assessed using Dunnett's multiple range test. Statistical significance was set at $P < 0.05$.

Author contributions

Ruixiang Luo, Ying Xu, and Zheng Jiang completed biological and cell-based assays. Ruixiang Luo, Jingjing Shao, Lulu Zheng, Jie Yu, and Linglan Tu participated in protein expression & purification, drug screening assay and *in vivo* antitumour study. Lin Ma, Sujuan Shuai, Zenghui Ye, and Jie Li synthesized the target compounds. Lin Ma and Weitao Fu completed the SBVS study. Lingfeng Chen proposed the project, performed data analysis and writing of the manuscript. Guang Liang, Xinting Lv, Yawen Zhang, Lina Yin, Lei Zheng contributed to the reviewing of the manuscript. All authors have given approval to the final version of the manuscript.

Declaration of competing interest

The authors declare the following financial interests/personal relationships which may be considered as potential competing interests: Lingfeng Chen reports financial support was provided by National Natural Science Foundation of China.

Data availability

Data will be made available on request.

Acknowledgments

This work was supported by the National Natural Science Foundation of China (82103999 to L.C.), Natural Science Funding of Zhejiang Province (LQ22H300007 to L.C.), Zhejiang Health Program (YS2022004 to LC), Zhejiang Medical and Health Science Project (2023KY622 to LZ), and Zhejiang Provincial Key Scientific Project (2021C03041 to G.L.).

Appendix A. Supplementary data

Supplementary data to this article can be found online at https://doi.org/10.1016/j.ejmech.2023.115305.

Abbreviations

DiFMUP	6,8-difluoro-4-methylumbelliferyl phosphate
EGFR	epidermal growth factor receptor
ERK	Ras-Raf-extracellular-signal-regulated kinase
GAB1	GRB2- associated-binding protein 1
HTS	high-throughput screening
IPTG	isopropyl ß-D-1-thiogalactopyranoside
IC50	half maximal inhibitory concentration
LMW-PTP	low-molecular-weight PTP
MAPK	mitogen-activated protein kinase
MD	molecular dynamic
NPs, PTP	protein tyrosine phosphatase
RTK	receptor tyrosine kinase
RMSDs	root mean square deviations
SAR	structure-activity relationship
SBVS	structure-based virtual screening
SHP2	Src homology 2 domain-containing phosphatase 2
TKIs	tyrosine kinases inhibitors

References

[1] R.J. Chan, G.S. Feng, PTPN11 is the first identified proto-oncogene that encodes a tyrosine phosphatase, Blood 109 (2007) 862–867.
[2] Y.N. Chen, M.J. LaMarche, H.M. Chan, P. Fekkes, J. Garcia-Fortanet, M.G. Acker, B. Antonakos, C.H. Chen, Z. Chen, V.G. Cooke, J.R. Dobson, Z. Deng, F. Fei, B. Firestone, M. Fodor, C. Fridrich, H. Gao, D. Grunenfelder, H.X. Hao, J. Jacob, S. Ho, K. Hsiao, Z.B. Kang, R. Karki, M. Kato, J. Larrow, L.R. La Bonte, F. Lenoir, G. Liu, S. Liu, D. Majumdar, M.J. Meyer, M. Palermo, L. Perez, M. Pu, E. Price, C. Quinn, S. Shakya, M.D. Shultz, J. Slisz, K. Venkatesan, P. Wang, M. Warmuth, S. Williams, G. Yang, J. Yuan, J.H. Zhang, P. Zhu, T. Ramsey, N.J. Keen, W. R. Sellers, T. Stams, P.D. Fortin, Allosteric inhibition of SHP2 phosphatase inhibits cancers driven by receptor tyrosine kinases, Nature 535 (2016) 148–152.
[3] T. Okazaki, S. Chikuma, Y. Iwai, S. Fagarasan, T. Honjo, A rheostat for immune responses: the unique properties of PD-1 and their advantages for clinical application, Nat. Immunol. 14 (2013) 1212–1218.
[4] A.D. Levy, X. Xiao, J.E. Shaw, S.P. Sudarsana Devi, S.M. Katrancha, A.M. Bennett, C.A. Greer, J.R. Howe, K. Machida, A.J. Koleske, Noonan syndrome-associated SHP2 dephosphorylates GluN2B to regulate NMDA receptor function, Cell Rep. 24 (2018) 1523–1535.
[5] M. Bentires-Alj, J.G. Paez, F.S. David, H. Keilhack, B. Halmos, K. Naoki, J.M. Maris, A. Richardson, A. Bardelli, D.J. Sugarbaker, W.G. Richards, J. Du, L. Girard, J. D. Minna, M.L. Loh, D.E. Fisher, V.E. Velculescu, B. Vogelstein, M. Meyerson, W. R. Sellers, B.G. Neel, Activating mutations of the noonan syndrome-associated SHP2/PTPN11 gene in human solid tumors and adult acute myelogenous leukemia, Cancer Res. 64 (2004) 8816–8820.
[6] X. Yuan, H. Bu, J. Zhou, C.Y. Yang, H. Zhang, Recent advances of SHP2 inhibitors in cancer therapy: current development and clinical application, J. Med. Chem. 63 (2020) 11368–11396.
[7] Z. Song, M. Wang, Y. Ge, X.P. Chen, Z. Xu, Y. Sun, X.F. Xiong, Tyrosine phosphatase SHP2 inhibitors in tumor-targeted therapies, Acta Pharm. Sin. B 11 (2021) 13–29.
[8] R.J. Nichols, F. Haderk, C. Stahlhut, C.J. Schulze, G. Hemmati, D. Wildes, C. Tzitzilonis, K. Mordec, A. Marquez, J. Romero, T. Hsieh, A. Zaman, V. Olivas, C. McCoach, C.M. Blakely, Z. Wang, G. Kiss, E.S. Koltun, A.L. Gill, M. Singh, M. A. Goldsmith, J.A.M. Smith, T.G. Bivona, RAS nucleotide cycling underlies the SHP2 phosphatase dependence of mutant BRAF-, NF1- and RAS-driven cancers, Nat. Cell Biol. 20 (2018) 1064–1073.
[9] P. Hof, S. Pluskey, S. Dhe-Paganon, M.J. Eck, S.E. Shoelson, Crystal structure of the tyrosine phosphatase SHP-2, Cell 92 (1998) 441–450.
[10] J.R. LaRochelle, M. Fodor, V. Vemulapalli, M. Mohseni, P. Wang, T. Stams, M. J. LaMarche, R. Chopra, M.G. Acker, S.C. Blacklow, Structural reorganization of SHP2 by oncogenic mutations and implications for oncoprotein resistance to allosteric inhibition, Nat. Commun. 9 (2018) 4508.
[11] L. Chen, S.S. Sung, M.L. Yip, H.R. Lawrence, Y. Ren, W.C. Guida, S.M. Sebti, N. J. Lawrence, J. Wu, Discovery of a novel shp2 protein tyrosine phosphatase inhibitor, Mol. Pharmacol. 70 (2006) 562–570.
[12] R. He, Z.H. Yu, R.Y. Zhang, L. Wu, A.M. Gunawan, B.S. Lane, J.S. Shim, L.F. Zeng, Y. He, L. Chen, C.D. Wells, J.O. Liu, Z.Y. Zhang, Exploring the existing drug space for novel pTyr mimetic and SHP2 inhibitors, ACS Med. Chem. Lett. 6 (2015) 782–786.
[13] M. Fodor, E. Price, P. Wang, H. Lu, A. Argintaru, Z. Chen, M. Glick, H.X. Hao, M. Kato, R. Koenig, J.R. LaRochelle, G. Liu, E. McNeill, D. Majumdar, G. A. Nishiguchi, L.B. Perez, G. Paris, C.M. Quinn, T. Ramsey, M. Sendzik, M. D. Shultz, S.L. Williams, T. Stams, S.C. Blacklow, M.G. Acker, M.J. LaMarche, Dual allosteric inhibition of SHP2 phosphatase, ACS Chem. Biol. 13 (2018) 647–656.
[14] M.J. LaMarche, M. Acker, A. Argintaru, D. Bauer, J. Boisclair, H. Chan, C.H. Chen, Y.N. Chen, Z. Chen, Z. Deng, M. Dore, D. Dunstan, J. Fan, P. Fekkes, B. Firestone, M. Fodor, J. Garcia-Fortanet, P.D. Fortin, C. Fridrich, J. Giraldes, M. Glick, D. Grunenfelder, H.X. Hao, M. Hentemann, S. Ho, A. Jouk, Z.B. Kang, R. Karki, M. Kato, N. Keen, R. Koenig, L.R. LaBonte, J. Larrow, G. Liu, S. Liu, D. Majumdar, S. Mathieu, M.J. Meyer, M. Mohseni, R. Ntaganda, M. Palermo, L. Perez, M. Pu, T. Ramsey, J. Reilly, P. Sarver, W.R. Sellers, M. Sendzik, M.D. Shultz, J. Slisz, K. Slocum, T. Smith, S. Spence, T. Stams, C. Straub, V. Tamez Jr., B.B. Toure, C. Towler, P. Wang, H. Wang, S.L. Williams, F. Yang, B. Yu, J.H. Zhang, S. Zhu, Identification of TNO155, an allosteric SHP2 inhibitor for the treatment of cancer, J. Med. Chem. 63 (2020) 13578–13594.
[15] D. Shen, W. Chen, J. Zhu, G. Wu, R. Shen, M. Xi, H. Sun, Therapeutic potential of targeting SHP2 in human developmental disorders and cancers, Eur. J. Med. Chem. 190 (2020), 112117.
[16] Z. Wang, H. Sun, C. Shen, X. Hu, J. Gao, D. Li, D. Cao, T. Hou, Combined strategies in structure-based virtual screening, Phys. Chem. Chem. Phys. 22 (2020) 3149–3159.
[17] D. Li, W. Zhou, J. Pang, Q. Tang, B. Zhong, C. Shen, L. Xiao, T. Hou, A magic drug target: androgen receptor, Med. Res. Rev. 39 (2019) 1485–1514.
[18] W. Fu, E. Wang, D. Ke, H. Yang, L. Chen, J. Shao, X. Hu, L. Xu, N. Liu, T. Hou, Discovery of a novel Fusarium graminearum mitogen-activated protein kinase (FgGpmk1) inhibitor for the treatment of Fusarium head blight, J. Med. Chem. 64 (2021) 13841–13852.
[19] W. Fu, M. Zhang, J. Liao, Q. Tang, Y. Lei, Z. Gong, L. Shan, M. Duan, X. Chai, J. Pang, C. Tang, X. Wang, X. Xu, D. Li, R. Sheng, T. Hou, Discovery of a novel androgen receptor antagonist manifesting evidence to disrupt the dimerization of the ligand-binding domain via attenuating the hydrogen-bonding network between the two monomers, J. Med. Chem. 64 (2021) 17221–17238.
[20] R.A.P. Padua, Y. Sun, I. Marko, W. Pitsawong, J.B. Stiller, R. Otten, D. Kern, Mechanism of activating mutations and allosteric drug inhibition of the phosphatase SHP2, Nat. Commun. 9 (2018) 4507.
[21] E. Wang, W. Fu, D. Jiang, H. Sun, J. Wang, X. Zhang, G. Weng, H. Liu, P. Tao, T. Hou, VAD-MM/GBSA: a variable atomic dielectric MM/GBSA model for improved accuracy in protein-ligand binding free energy calculations, J. Chem. Inf. Model. 61 (2021) 2844–2856.
[22] L. Chen, W. Fu, L. Zheng, Z. Liu, G. Liang, Recent progress of small-molecule epidermal growth factor receptor (EGFR) inhibitors against C797S resistance in non-small-cell lung cancer, J. Med. Chem. 61 (2018) 4290–4300.
[23] X. Lu, L. Yu, Z. Zhang, X. Ren, J.B. Smaill, K. Ding, Targeting EGFR(L858R/T790M) and EGFR(L858R/T790M/C797S) resistance mutations in NSCLC: current developments in medicinal chemistry, Med. Res. Rev. 38 (2018) 1550–1581.
[24] L.S. Lock, I. Royal, M.A. Naujokas, M. Park, Identification of an atypical Grb2 carboxyl-terminal SH3 domain binding site in Gab docking proteins reveals Grb2-dependent and -independent recruitment of Gab1 to receptor tyrosine kinases, J. Biol. Chem. 275 (2000) 31536–31545.
[25] F. Sacco, L. Perfetto, L. Castagnoli, G. Cesareni, The human phosphatase interactome: an intricate family portrait, FEBS Lett. 586 (2012) 2732–2739.
[26] J. Liddle, F.L. Atkinson, M.D. Barker, P.S. Carter, N.R. Curtis, R.P. Davis, C. Douault, M.C. Dickson, D. Elwes, N.S. Garton, M. Gray, T.G. Hayhow, C. I. Hobbs, E. Jones, S. Leach, K. Leavens, H.D. Lewis, S. McCleary, M. Neu, V. K. Patel, A.G. Preston, C. Ramirez-Molina, T.J. Shipley, P.A. Skone, N. Smithers, D. O. Somers, A.L. Walker, R.J. Watson, G.G. Weingarten, Discovery of GSK143, a highly potent, selective and orally efficacious spleen tyrosine kinase inhibitor, Bioorg. Med. Chem. Lett. 21 (2011) 6188–6194.
[27] G. Coffey, A. Betz, F. DeGuzman, Y. Pak, M. Inagaki, D.C. Baker, S.J. Hollenbach, A. Pandey, U. Sinha, The novel kinase inhibitor PRT062070 (Cerdulatinib) demonstrates efficacy in models of autoimmunity and B-cell cancer, J. Pharmacol. Exp. Therapeut. 351 (2014) 538–548.
[28] Y. Liu, X. Yang, Y. Wang, Y. Yang, D. Sun, H. Li, L. Chen, Targeting SHP2 as a therapeutic strategy for inflammatory diseases, Eur. J. Med. Chem. 214 (2021), 113264.
[29] B.G. Neel, H. Gu, L. Pao, The `Shp'ing news: SH2 domain-containing tyrosine phosphatases in cell signaling, Trends Biochem. Sci. 28 (2003) 284–293.
[30] M. Zhao, W. Guo, Y. Wu, C. Yang, L. Zhong, G. Deng, Y. Zhu, W. Liu, Y. Gu, Y. Lu, L. Kong, X. Meng, Q. Xu, Y. Sun, SHP2 inhibition triggers anti-tumor immunity and synergizes with PD-1 blockade, Acta Pharm. Sin. B 9 (2019) 304–315.
[31] M. Marasco, A. Berteotti, J. Weyershaeuser, N. Thorausch, J. Sikorska, J. Krausze, H.J. Brandt, J. Kirkpatrick, P. Rios, W.W. Schamel, M. Kohn, T. Carlomagno,

Molecular mechanism of SHP2 activation by PD-1 stimulation, Sci. Adv. 6 (2020), eaay4458.
[32] Y. Song, S. Wang, M. Zhao, X. Yang, B. Yu, Strategies targeting protein tyrosine phosphatase SHP2 for cancer therapy, J. Med. Chem. 65 (2022) 3066–3079.
[33] J.M. Cunnick, J.F. Dorsey, T. Munoz-Antonia, L. Mei, J. Wu, Requirement of SHP2 binding to Grb2-associated binder-1 for mitogen-activated protein kinase activation in response to lysophosphatidic acid and epidermal growth factor, J. Biol. Chem. 275 (2000) 13842–13848.
[34] T.S. Batth, M. Papetti, A. Pfeiffer, M.A.X. Tollenaere, C. Francavilla, J.V. Olsen, Large-scale phosphoproteomics reveals shp-2 phosphatase-dependent regulators of pdgf receptor signaling, Cell Rep. 22 (2018) 2784–2796.
[35] M. Liu, S. Gao, R.M. Elhassan, X. Hou, H. Fang, Strategies to overcome drug resistance using SHP2 inhibitors, Acta Pharm. Sin. B 11 (2021) 3908–3924.
[36] R. Paccoud, C. Saint-Laurent, E. Piccolo, M. Tajan, A. Dortignac, O. Pereira, S. Le Gonidec, I. Baba, A. Gelineau, H. Askia, M. Branchereau, J. Charpentier, J. Personnaz, S. Branka, J. Auriau, S. Deleruyelle, M. Canouil, N. Beton, J.P. Salles, M. Tauber, J. Weill, P. Froguel, B.G. Neel, T. Araki, C. Heymes, R. Burcelin, I. Castan, P. Valet, C. Dray, E.L. Gautier, T. Edouard, J.P. Pradere, A. Yart, SHP2 drives inflammation-triggered insulin resistance by reshaping tissue macrophage populations, Sci. Transl. Med. 13 (2021).
[37] Q. Liu, J. Qu, M. Zhao, Q. Xu, Y. Sun, Targeting SHP2 as a promising strategy for cancer immunotherapy, Pharmacol. Res. 152 (2020), 104595.
[38] C.A. Eberlein, D. Stetson, A.A. Markovets, K.J. Al-Kadhimi, Z. Lai, P.R. Fisher, C. B. Meador, P. Spitzler, E. Ichihara, S.J. Ross, M.J. Ahdesmaki, A. Ahmed, L. E. Ratcliffe, E.L. O'Brien, C.H. Barnes, H. Brown, P.D. Smith, J.R. Dry, G. Beran, K. S. Thress, B. Dougherty, W. Pao, D.A. Cross, Acquired resistance to the mutant-selective EGFR inhibitor AZD9291 is associated with increased dependence on RAS signaling in preclinical models, Cancer Res. 75 (2015) 2489–2500.

Vol. 233 • 5 April 2022 • ISSN 0223-5234

ELSEVIER

EUROPEAN JOURNAL OF MEDICINAL CHEMISTRY

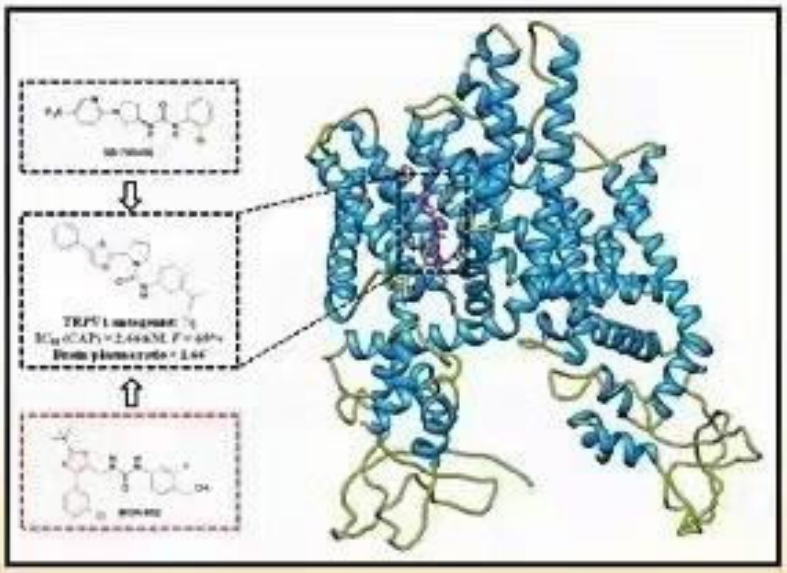

Clarivate™ Web of Science™

经检索《Web of ScienceTM 核心合集》和《Journal Citation Reports，JCR》以及中科院分区表，下列论文被《Sci-Expanded》收录（检索时间 2023/11/07）。

他引文献数来自 Web of Science 核心合集 引文索引：Science Citation Index Expanded(SCI-EXPANDED)--1999-至今

文献类型:Article

标题:Discovery of a potent and selective allosteric inhibitor targeting the SHP2 tunnel site for RTK-driven cancer treatment

作者:Luo, RX(Luo, Ruixiang)Fu, WT(Fu, Weitao)Shao, JJ(Shao, Jingjing)Ma, L(Ma, Lin)Shuai, SJ(Shuai, Sujuan)Xu, Y(Xu, Ying)Jiang, Z(Jiang, Zheng)Ye, ZH(Ye, Zenghui)Zheng, LL(Zheng, Lulu)Zheng, L(Zheng, Lei)Yu, J(Yu, Jie)Zhang, YW(Zhang, Yawen)Yin, LA(Yin, Lina)Tu, LL(Tu, Linglan)Lv, XT(Lv, Xinting)Li, J(Li, Jie)Liang, G(Liang, Guang)Chen, LF(Chen, Lingfeng)

来源出版物:EUROPEAN JOURNAL OF MEDICINAL CHEMISTRY 卷:253

DOI:10.1016/j.ejmech.2023.115305 出版时间:MAY 5 2023 在线发表:APR 2023 已索引:2023-05-06

入藏号:WOS:000975737700001　　PubMed ID:37023678　　文献号:115305

来自 Web of Science 核心合集的被引频次:0 所有数据库的被引频次:0　　他引:0

地址：[Luo, Ruixiang;Shao, Jingjing;Ma, Lin;Xu, Ying;Jiang, Zheng;Ye, Zenghui;Zheng, Lei;Yu, Jie;Zhang, Yawen;Yin, Lina;Tu, Linglan;Lv, Xinting;Li, Jie;Liang, Guang;Chen, Lingfeng]Hangzhou Med Coll, Affiliated Yongkang Peoples Hosp 1, Hangzhou 310012, Zhejiang, Peoples R China

[Luo, Ruixiang;Shao, Jingjing;Ma, Lin;Xu, Ying;Jiang, Zheng;Ye, Zenghui;Zheng, Lei;Yu, Jie;Zhang, Yawen;Yin, Lina;Tu, Linglan;Lv, Xinting;Li, Jie;Liang, Guang;Chen, Lingfeng]Hangzhou Med Coll, Sch Pharm, Hangzhou 310012, Zhejiang, Peoples R China

[Fu, Weitao]Jiangsu Vcare PharmaTech Co Ltd, Dept Comp Aided Drug Design, Nanjing 211800, Peoples R China

[Shao, Jingjing;Liang, Guang]Wenzhou Med Univ, Sch Pharmaceut Sci, Wenzhou 325035, Zhejiang, Peoples R China

[Shuai, Sujuan;Li, Jie]Sch Med, Zhejiang Univ City Coll, Dept Pharm, Hangzhou 310015, Peoples R China

[Zheng, Lulu]Tongde Hosp Zhejiang Prov, Dept Pharm, Hangzhou 310000, Zhejiang, Peoples R China

[Liang, Guang;Chen, Lingfeng]Hangzhou Med Coll, Sch Pharmaceut Sci, Hangzhou 310012, Peoples R China

[Li, Jie]Zhejiang Univ City Coll, Sch Pharmaceut Sci, Hangzhou 310015, Peoples R China

通讯作者地址:Li, Jie;Liang, Guang;Chen, Lingfeng (通讯作者),Hangzhou Med Coll, Affiliated Yongkang Peoples Hosp 1, Hangzhou 310012, Zhejiang, Peoples R China.Liang, Guang;Chen, Lingfeng (通讯作者),Hangzhou Med Coll, Sch Pharmaceut Sci, Hangzhou 310012, Peoples R China.Li, Jie (通讯作者),Zhejiang Univ City Coll, Sch Pharmaceut Sci, Hangzhou 310015, Peoples R China.

电子邮件地址：lijie@zucc.edu.cn;wzmcliangguang@163.com;lfchen@hmc.edu.cn

ISSN:0223-5234 eISSN:1768-3254

期刊《EUROPEAN JOURNAL OF MEDICINAL CHEMISTRY》2022 年的 JCR 影响因子为：6.7，五年期刊影响因子:6.5。

2022 年该刊在中科院分区(升级版)：

	学科名称	分区	Top 期刊
大类	医学	1	是
小类	CHEMISTRY, MEDICINAL 药物化学	1	-

注：以上检索结果均得到被检索人的确认。

温州医科大学图书馆（盖章）

检索日期：2023-11-07

2022年期刊分区表升级版

2022年12月21日发布

EUROPEAN JOURNAL OF MEDICINAL CHEMISTRY

ISSN: 0223-5234

Review: 否

大类及分区

医学 1 区 Top

小类及分区

CHEMISTRY, MEDICINAL 药物化学 1 区

附件：

杭州医学院学术论文投稿登记单

登记日期：

论文作者所在二级学院（部）：

论文类型：〔√〕研究论文〔 〕综述〔 〕会议论文〔 〕其他：

论文作者：Ruixiang Luo#, Weitao Fu#, Jingjing Shao #, Lin Ma#, Sujuan Shuai, Ying Xu, Zheng Jiang, Zenghui Ye, Lulu Zheng, Lei Zheng, Jie Yu, Yawen Zhang, Lina Yin, Linglan Tu, Xinting Lv, Jie Li a,d*, Guang Liang*, Lingfeng Chen*

论文标题：Discovery of a potent and selective allosteric inhibitor targeting the SHP2 tunnel site for RTK-driven cancer treatment

投稿期刊：European Journal of Medicinal Chemistry

资助项目及其编号：国家自然科学基金，82103999

浙江省自然基金，LQ22H300007

医药卫生计划，2023KY622

浙江省卫生计划，YS2022004

浙江省重大研发项目，2021C03041

论文作者及其签名（My signature below constitutes consent for release of the above-cited manuscript for publication and certifies that the information contained therein is suitable for publication）：（外

籍填写护照号）

第一作者：[redacted] 身份证号：440106199907121814 日期：2023.11.29

付伟涛 身份证号：330102199706261014 日期：2023.11.29

邬静静 身份证号：330327200008228405 日期：2023.11.29

马琳 身份证号：140108199704254819 日期：2023.11.29

通讯作者：李杰 身份证号：330381199110170011 日期：20231129

[redacted] 身份证号：430181198112210812 日期：2023.11.29

[redacted] 身份证号：330382199202123253 日期：2023.11.29

其他作者：仲秀娟 身份证号：330781199609112402 日期：2023.1129

许颖 身份证号：331002200004172801 日期：2023.11.29

姜征 身份证号：220106199909108444X 日期：2023.11.29

叶蕾萍 身份证号：331002199403272512 日期：2023.11.29

郑瑶瑶 身份证号：330328199202082308 日期：2023.11.29

郑雷 身份证号：330106199305090010 日期：20231129

于浩 身份证号：330522199701133302 日期：20231127

张雅雯 身份证号：330503198402028308 日期：2023.11.29

尹丽娜 身份证号：330623198210173584 日期：2023.11.29

屠凌岚 身份证号：331102198912207103 日期：2023.1129

本篇论文内容符合国家法律、社会公德，不违反科研伦理；论文内容无捏造和篡改研究结果、实验数据，无剽窃他人的研究成果；论文中引用资料、文献，均已详加注释和说明，无涉密资料的文献且本论文投稿已征得以上各作者同意；若本承诺书为代签，已征得第一/通讯作者同意。

承诺人：陈志辉

日期：2023.11.29

（如代第一/通讯作者签名，请注明原因）